

# Giant Radio Sources in View of the Dynamical Evolution of FRII-type Population. I. The Observational Data, and Basic Physical Parameters of Sources Derived from the Analytical Model

by

J. Machalski, K.T. Chyży & M. Jamrozy

Astronomical Observatory, Jagellonian University, ul. Orła 171,  
30-244 Cracow, Poland

e-mail: machalsk@oa.uj.edu.pl jamrozy@oa.uj.edu.pl

## Abstract

The time evolution of *giant* lobe-dominated radio galaxies (with projected linear size  $D > 1$  Mpc if  $H_0=50 \text{ km s}^{-1}\text{Mpc}^{-1}$  and  $q_0=0.5$ ) is analysed on the basis of dynamical evolution of the entire FRII-type population. Two basic physical parameters, namely the jet power  $Q_0$  and central density of the galaxy nucleus  $\rho_0$  are derived for a sample of *giants* with synchrotron ages reliably determined, and compared with the relevant parameters in a comparison sample of normal-size sources consisting of 3C, B2, and other sources. Having the apparent radio luminosity  $P$  and linear size  $D$  of each sample source,  $Q_0$  and  $\rho_0$  are obtained by fitting the dynamical model of Kaiser et al. (1997). We find that: (i) there is not a unique factor governing the source size; they are old sources with temperate jet power ( $Q_0$ ) evolved in a relatively low-density environment ( $\rho_0$ ). The size is dependent, in order of decreasing partial correlation coefficients, on age; then on  $Q_0$ ; next on  $\rho_0$ . (ii) A self-similar expansion of the sources' cocoon seems to be feasible if the power supplied by the jets is a few orders of magnitude above the minimum-energy value. In other cases the expansion can only initially be self-similar; a departure from self-similarity for large and old sources is justified by observational data of *giant* sources. (iii) An apparent increase of the lowest internal pressure value observed within the largest sources' cocoon with redshift is obscured by the intrinsic dependence of their size on age and the age on redshift, which hinders us from making definite conclusions about a cosmological evolution of intergalactic medium (IGM) pressure.

**Key words:** galaxies: active – galaxies: evolution – galaxies: kinematics and dynamics

## 1 Introduction

Extragalactic radio sources, powered by twin jets resulting from nuclear energy processes in the Active Galactic Nucleus (AGN), exhibit a very large

range of their linear size. The sizes of these powerful sources range from less than  $10^2$  pc (GPS: Giga Hertz-peaked spectrum), to  $10^2 - 10^4$  pc (CSS: compact steep spectrum),  $10^4 - 10^6$  pc (normal-size sources), up to greater than  $10^6$  pc  $\equiv$  1 Mpc ('giant' radio sources). One of the key problems of the evolution of extragalactic sources is whether and how different size sources are related. Is there a single evolutionary scheme governing the size evolution of radio sources, or do small and large sources evolve in a different way?

From many years 'giant'<sup>1</sup> radio sources have been of special interest for several reasons. Their very large angular sizes give excellent opportunity for the study of source physics. They are also very useful to study the density and evolution of the intergalactic and intracluster environment (cf. Subrahmanyan and Saripalli 1993; Mack et al. 1998), as well as to verify the unification scheme for powerful radio sources (Barthel 1989; Urry and Padovani 1995). Finally, they can be used to constrain dynamical models of the source lifetime evolution (e.g. Kaiser and Alexander 1999). The general questions are: do the largest radio sources reach their extremal *giant* sizes due to (i) exceptional physical conditions in the intergalactic medium, (ii) extraordinary intrinsic properties of the AGN, or simply (iii) because they are extremely old?

To answer these questions, in a number of papers attempts were made to recognize properties other than size which may differentiate *giants* from normal-size sources. The *giant*-source morphologies, energy density in the lobes and interaction with the intergalactic medium were studied by Subrahmanyan et al. (1996), who suggested that *giant* radio galaxies may be located in the lowest density regions, and 'may attained their large size as a result of restarting of their central engines in multiple phases of activity along roughly similar directions'. Also Mack et al. (1998), after a study of 5 nearby *giant* radio galaxies, argued that those sources are so huge because of their low-density environment and not because of their old ages. A similar conclusion was drawn by Cotter (1998) after his study of a sample of high-redshift 7C giants. He found those sources to be not old and of similar kinetic powers of the jet as normal-size 3C sources. But the densities of their surrounding medium was found to be much lower than those around most of 3C sources (Rawlings and Saunders 1991). Ishwara-Chandra and Saikia (1999) compiled a sample of more than 50 known *giant* sources (many of them being of FRI-type morphology) and compared some of their properties with those of a complete sample of 3CR sources 'to investigate the evolution of giant sources, and test their consistency with the unified scheme for radio galaxies and quasars'. They concluded that the location of *giants* on the

---

<sup>1</sup>hereafter we use *giant* or *giants* instead of giant radio source(s)

power–linear size ( $P - D$ ) diagram may suggest that the largest sources have evolved from the smaller sources. Finally, in the recent extensive study of 26 *giant* galaxies by Schoenmakers et al. (2000), the authors argued that those galaxies ‘are both old sources, in term of their spectral age, and are situated in a relatively low-density environment, but also that neither of these two properties are extreme. Therefore, their large size probably results from a combination of these properties’.

From the above results, it is clear that the phenomenon of the *giant* radio sources is still open to further research. Therefore, in this paper we analyse whether observed properties of *giant* sources can be explained by a model of the dynamical evolution of classical double radio sources in cosmic time, and what factor (if there is a one) is primarily responsible for the *giant* size. Obviously such an analysis, based on the giant radio sources only, i.e. the sources with a strongly limited range of linear sizes, would not be reliable and even possible. Therefore, to solve the above problems we analyse the sample of radio sources comprising both the ‘giant’-size and ‘normal’-size sources, most of the latter with sizes from  $\sim 100$  kpc to 1 Mpc.

Most published analytical models of the dynamical evolution of extended powerful radio sources are based on the hydrodynamical self-similar expansion of the sources’ cocoon caused by the interaction of light and supersonic jets with the ambient medium. Carvalho and O’Dea (2002) classify those models into three mutually exclusive types encoded as I, II, and III, and give an excellent description of their properties. However, we realize that only few of them deal with the source’s energetics and the radio luminosity evolution with time which is crucial for e.g. the analysis of evolutionary tracks of sources on the luminosity–size ( $P - D$ ) plane, i.e. the most sensitive characteristics of the dynamical models.

Two type III models, published by Kaiser, Dennett-Thorpe and Alexander (1997) [hereafter referred to as KDA] and Blundell, Rawlings and Willott (1999) [hereafter BRW], are more sophisticated than models of type I and II. We apply the KDA model for its simplicity in comparison with the BRW one, and in spite of some objections about an application of the self-similar models to large and old sources in which an internal pressure cannot be always above the external medium pressure (e.g. Hardcastle and Worrall 2000).

The present analysis is confined to classical double radio sources with FRII-type (Fanaroff and Riley 1974) morphology. Synchrotron ages in a sample comprising both giant and normal-size sources are used to verify the dynamical time evolution of such sources predicted by the above analytical model. Basic physical parameters, i.e. the jet power  $Q_0$ , the central density of the galaxy nucleus  $\rho_0$ , the energy density and pressure in the lobes/cocoon ( $u_c$  and  $p_c$ ), and the total energy of the source  $E_{\text{tot}}$  are derived with the

KDA model for each member of the sample to fit its estimated age, redshift, monochromatic radio luminosity, projected size, and axial ratio. Besides, the fitted values of some of these parameters are directly compared with the relevant values calculated straight from the data, e.g. the equipartition magnetic field strength,  $B_{\text{eq}}$ , equipartition energy density in the source,  $u_{\text{eq}}$ , and its total energy  $U_{\text{eq}}$ . These ‘observational’ values and their errors are homogeneously calculated using the method outlined by Miley (1980). Next, the physical parameters derived for real radio sources are used to specify the conditions or circumstances under which the FR II-type radio sources can reach the largest observed linear sizes, to verify the applicability of the self-similar analytical models for the largest sources, and to search for an evidence after a cosmological evolution of the ambient pressure in the intergalactic medium (IGM).

The observational data used and the physical parameters of the sample sources found directly from the data are given in Section 2. The application of the dynamical models is described in Section 3, while in Section 4 results of the modelling are presented in the form of statistically significant correlations between physical parameters of the sample sources derived from the fitting procedure and their apparent observational parameters. The results obtained are discussed in Section 5 and the conclusions are given in Section 6.

## 2 Observational Data

### 2.1 Selection Criteria

Similarly to the approach of Ishwara-Chandra and Saikia, we have compiled a subsample of 18 *giant* sources and a comparison subsample of 54 normal-size sources. The selection criteria were as follows: (i) the sources have the FR II-type morphology, (ii) The existing radio maps enable a suitable determination of their lateral extend, i.e. transversal to the source’s axis, and (iii) their spectral age or the expansion velocity, determined with the same model of the energy losses, are available from the literature. The spectral ageing data calculated with the JP model (Jaffe and Perola 1973; cf. Sect. 2.4) for the *giants* are taken from the papers of Saripalli et al. (1994), Parma et al. (1996), Mack et al. (1998), Schoenmakers et al. (1998, 2000), Ishwara-Chandra and Saikia (1999), Lara et al. (2000), and Machalski and Jamrozy (2000). For the aim of this paper, i.e. for an observational verification of the dynamical time evolution of classical radio sources, especially the growth of their linear size with time predicted by the analytical models, the comparison subsample has been chosen to comprise high-luminosity (high- and low-redshift), as well as low-luminosity normal-size sources. The high-redshift

(with  $z \geq 0.5$ ) and low-redshift ( $z < 0.5$ ) sets consist of 3C sources taken from the papers of Alexander and Leahy (1987), Leahy et al. (1989), Liu et al. (1992), and Guerra et al. (2000). All of them have  $P_{178} \geq 10^{25} \text{ W Hz}^{-1} \text{ sr}^{-1}$  (other selection criteria are summarized in Liu et al.). The low-luminosity set comprises FRII-type sources with  $P_{1.4} < 10^{24.4} \text{ W Hz}^{-1} \text{ sr}^{-1}$  (corresponding to  $P_{178} < 10^{25} \text{ W Hz}^{-1} \text{ sr}^{-1}$  assuming a mean spectral index of 0.7 between 178 and 1400 MHz). A limited number of such sources with spectral ages determined have been available from the papers of Klein et al. (1995) and Parma et al. (1999).

## 2.2 Observational Parameters

For all individual sample sources the following observational parameters are determined: the redshift  $z$ , the 1.4 GHz luminosity in  $\text{W Hz}^{-1} \text{ sr}^{-1}$ , the projected linear size  $D$  in kpc, the cocoon's axial ratio  $AR = D/b$  and volume  $V_o$  in  $\text{kpc}^3$ . The volume of the source,  $V_o$ , is calculated assuming a cylindrical geometry with the length  $D$ , and the base diameter  $b$  taken as the average of the full deconvolved widths of the two lobes. The latter are measured between  $3\sigma$  contours on a radio contour map half-way between the core and the hot spots or distinct extremities of the source. All these data for the *giant*-size and normal-size sources in our sample are given in columns 3–7 of Table 1. The columns 8–9 of Table 1 give the reference papers to the radio map used to determine both  $D$  and  $AR$  for each sample source and its spectral age, respectively.

## 2.3 Physical Parameters Derived Directly from the Data

As mentioned in Section 1, the equipartition magnetic field  $B_{\text{eq}}$ , the energy density  $u_{\text{eq}}$ , and the total emitted energy  $U_{\text{eq}}$  with their errors are calculated with the method outlined by Miley (1980). However, the Miley's assumption of pure power-law radio spectrum has been abandoned; the cocoon's radio spectrum has been determined by the least-square method fit of the simple analytic functions:  $y = a + bx + c \exp(\pm x)$  or  $y = a + bx + cx^2$  (where  $x = \log \nu [\text{GHz}]$ ,  $y = \log S(\nu)$ ) to the available flux densities  $S(\nu)$  weighted by their given error. The total luminosity of the cocoon has been then integrated between 10 MHz and 100 GHz using the above fitted spectrum with  $H_0 = 50 \text{ km s}^{-1} \text{ Mpc}^{-1}$  and  $q_0 = 0.5^2$ . The values of  $u_{\text{eq}}$ ,  $B_{\text{eq}}$ , and  $U_{\text{eq}} = u_{\text{eq}} V_o$  with

---

<sup>2</sup>An application of the most recent cosmological constants will change numerical values of dimensions, power, ambient density, etc., but not relations between observational and physical parameters of the sources. The applied constants provide an easier comparison of the derived physical parameters of sources with those found in a large number of previously

their estimated error, calculated for each of the sample sources with the assumption of a filling factor of unity and equipartition of energy between electrons and protons, are given in columns 3–5 of Table 2, respectively. Table 2 contains the adopted age and physical parameters of the sample sources derived either from the observational data (columns 3, 4, and 5) and from the analytical KDA model (columns 6, 7, 8, and 9).

## 2.4 Spectral Age

Determination of the age of the radio sources is crucial to constrain any dynamical model of their time evolution. An apparent age of sources can be estimated from the ratio of their total emitted energy,  $U_{\text{eq}}$ , determined under the ‘minimum energy’ condition and the observed power

$$t_{\text{max}} \approx U_{\text{eq}}/(dU/dt) \quad \text{where} \quad dU/dt \equiv \int_{\nu_1}^{\nu_2} S(\nu)d\nu,$$

and  $S(\nu)$  is the observed flux density at different frequencies. The resultant age of source, being rather its upper limit, is usually greater than the synchrotron age of relativistic particles commonly determined from the standard spectral-ageing analysis (e.g. Alexander and Leahy 1987). However, the time-dependence of various energy losses suffered by the particles causes different parts of the lobes or cocoon to have different ages. Besides, the radiation losses (and thus the synchrotron age) depend on the history of particle injection, the distribution of the pitch angle, etc. described by the different synchrotron models: Kardashev–Pacholczyk (KP); Jaffe and Perola (JP); or continuous injection (CI), cf. Carilli et al.(1991) for a detailed description. Therefore, these models of different energy losses give different spectral age estimates, and a comparison of ages of the sample sources ought to be made within the same synchrotron model. Moreover, the synchrotron ages ( $t_{\text{syn}}$ ) usually differ from the dynamical age ( $t_{\text{dyn}}$ ) estimated from the ram-pressure arguments (cf. Begelman and Cioffi 1989; Lara et al. 2000; Schoenmakers et al. 2000).

An attempt to minimize the discrepancies between spectral and dynamical ages has been undertaken by Kaiser (2000). His 3-dimensional model of the synchrotron emissivity of the cocoon traces the individual evolution of parts of the cocoon and provides, according to the author, a more accurate estimate for the age of a source. Its application to the lobes of Cygnus A gave a very good fit to their observed surface brightness distribution. However, since an application of the above model is confined to the sources for which their lobes are reasonably resolved in the direction perpendicular to

---

published papers

the jet axis – we cannot use it for our statistical approach to the dynamical evolution of *giant* radio sources and have to rely on results of the standard ageing analysis.

Basing on a commonly accepted assumption about the proportionality of the spectral and dynamical ages, hereafter we assume  $t_{\text{dyn}} = 2t_{\text{syn}}$  (e.g. Lara et al. 2000). This age (marked by  $t[\text{Myr}]$ ) is given in column 2 of Table 2.

### 3 Application of the KDA Model

#### 3.1 Source Dynamics

The overall dynamics of a FR II-type source (precisely: its cocoon) described in the KDA model is based on the earlier self-similar model of Kaiser and Alexander (1997) [hereafter referred to as KA]. It is assumed that the radio structure is formed by two jets emanating from the AGN into a surrounding medium in two opposite directions, then terminating in strong shocks, and finally inflating the cocoon. A density distribution of the unperturbed external gas is approximated by a power-law relation  $\rho_d = \rho_0(d/a_0)^{-\beta}$ , where  $d$  is the radial distance from the core of a source,  $\rho_0$  is the density at the core radius  $a_0$ , and  $\beta$  is the exponent in this distribution [the simplified King (1972) model].

Half of the cocoon is approximated by a cylinder of length  $L_j = D_s/2$  and axial ratio  $R_T = AR/2$ , where  $D_s$  is its total unprojected linear size. The cocoon expands along the jet axis driven by the hot spot pressure  $p_h$  and in the perpendicular direction by the cocoon pressure  $p_c$ . In the model the rate at which energy is transported along each jet ( $Q_0$ ) is constant during the source lifetime. The model predicts self-similar expansion of the cocoon and gives analytical formulae for the time evolution of various geometrical and physical parameters, e.g. the length of the jet [cf. equations (4) and (5) in KA]:

$$L_j = D_s/2 = c_1 \left( \frac{Q_0}{\rho_0 a_0^\beta} \right)^{1/(5-\beta)} t^{3/(5-\beta)}; \quad (1)$$

and the cocoon pressure (cf. equation 34 in KA):

$$p_c = \frac{18c_1^{2(5-\beta)/3}}{(\Gamma_x + 1)(5 - \beta)^2 \mathcal{P}_{\text{hc}}} (\rho_0 a_0^\beta Q_0^2)^{1/3} L_j^{-(4+\beta)/3}, \quad (2)$$

where  $c_1$  is a dimensionless constant [equation (25) in KA], and  $\Gamma_x$  is the adiabatic index of the unshocked medium surrounding the cocoon, and  $\mathcal{P}_{\text{hc}} \equiv p_h/p_c$  is the pressure ratio.

However, the pressure ratio  $\mathcal{P}_{\text{hc}} = 4R_{\text{T}}^2$ , implied in the original KDA paper, has later been found to seriously overestimate the value of  $\mathcal{P}_{\text{hc}}$  obtained in hydrodynamical simulations by Kaiser and Alexander (1999). Therefore, in our modelling procedure we use the empirical formula taken from Kaiser (2000):

$$\mathcal{P}_{\text{hc}} = (2.14 - 0.52\beta)R_{\text{T}}^{2.04-0.25\beta}. \quad (3)$$

### 3.2 Source Energetics and Radio Power

In our application of the KDA model we neglect thermal particles, hence the overall source dynamics is governed by the pressure in the cocoon in the form  $p_{\text{c}} = (\Gamma_{\text{c}} - 1)(u_{\text{e}} + u_{\text{B}})$ , where  $\Gamma_{\text{c}}$  is the adiabatic index of the cocoon,  $u_{\text{e}}$  and  $u_{\text{B}}$  are the energy densities of relativistic particles and the magnetic field, respectively. Both energy densities are a function of the source lifetime  $t$ . In particular,

$$u_{\text{B}}(t) \propto B^2(t) = \text{const } t^{-a}, \quad (4)$$

where  $a = (\Gamma_{\text{B}}/\Gamma_{\text{c}})(4 + \beta)/(5 - \beta)$ .

Since the time evolution of the pressure  $p_{\text{c}}$  is known from the self-similar solution, then one can calculate the energy density in the cocoon at any specific age  $t$ :

$$u_{\text{c}}(t) \equiv u_{\text{e}}(t) + u_{\text{B}}(t) = p_{\text{c}}(t)/(\Gamma_{\text{c}} - 1), \quad (5)$$

and the total source energy:  $E_{\text{tot}}(t) = u_{\text{c}}(t)V_{\text{c}}(t)$ , where  $V_{\text{c}}$  is the cocoon volume attained at the age  $t$ :

$$V_{\text{c}}(t) = 2\frac{\pi}{4R_{\text{T}}^2}[L_{\text{j}}(t)]^3 \propto t^{9/(5-\beta)}. \quad (6)$$

Following KDA and Kaiser (2000) we can write:

$$E_{\text{tot}} = u_{\text{c}}V_{\text{c}} = \frac{2(5 - \beta)}{9[\Gamma_{\text{c}} + (\Gamma_{\text{c}} - 1)(\mathcal{P}_{\text{hc}}/4)] - 4 - \beta}Q_0t. \quad (7)$$

Thus, the ratio of energy delivered by the twin jets and stored in the cocoon is:

$$\frac{2Q_0t}{E_{\text{tot}}} = \frac{9\Gamma_{\text{c}} - 4 - \beta}{5 - \beta} + \frac{9(\Gamma_{\text{c}} - 1)}{4(5 - \beta)}\mathcal{P}_{\text{hc}},$$

i.e. for given  $\Gamma_{\text{c}}$  and  $\beta$  values, this ratio is a function of the pressure ratio  $\mathcal{P}_{\text{hc}}$  only. For  $\Gamma_{\text{c}} = 5/3$  and  $\beta = 3/2$  we have

$$2Q_0t/E_{\text{tot}} = 2.7 + 0.43\mathcal{P}_{\text{hc}}. \quad (8)$$

The radio power of the cocoon  $P_\nu$  is calculated in the KDA model by splitting up the source into small volume elements and allowing them to evolve separately. The effects of adiabatic expansion, synchrotron losses, and inverse Compton scattering on the cosmic microwave background radiation are traced for these volume elements independently. The total radio emission at a fixed frequency  $\nu$  is then obtained by summing up the contribution from all such elements, resulting in an integral over time [equation (16) in KDA]. It depends on the source’s age  $t$  and redshift  $z$ , the jet power  $Q_0$ , the cocoon axial ratio  $R_T$ , the exponent in the expected power-law distribution of relativistic particles  $p$ , and on the ratio  $r$  of the magnetic field energy to the energy of relativistic electrons and non-radiating particles (given in Sect. 3.3). The integral is not analytically solvable and, following the KDA we calculate it numerically.

### 3.3 Fitting Procedure

On the basis of the above model we aim to predict the specific physical parameters for all *giants* and normal-size sources in the sample at their estimated (dynamical) age, i.e.  $Q_0$ ,  $\rho_0$ ,  $u_c$ ,  $p_c$ , and  $E_{\text{tot}}$ . This differs from the KDA approach, who on the base of available observational data, evaluated some general trends and made crude estimates of possible ranges of values attained by the model parameters.

In order to derive the above parameters for our sources, all other free parameters of the model ( $r$ ,  $p$ ,  $\Gamma_x$ ,  $\Gamma_c$ ,  $\Gamma_B$ ,  $a_0$ ,  $\beta$ ), and the inclination angle of the jet axis to the observer’s line-of-sight  $\theta$  have to be approximated. Following the KDA, we adopt their ‘Case 3’ where both the cocoon and magnetic field are ‘cold’ ( $\Gamma_c = \Gamma_B = 5/3$ ) and the adiabatic index of the jet material and external gas is also 5/3. For the initial ratio of the energy densities of the magnetic field and the particles we use  $r \equiv u_B/u_e = (1+p)/4$ , with the exponent of the energy distribution  $p = 2.14$ .

The core radius  $a_0$  is one of the most difficult model parameter to be set up. Even careful 2-D modelling of a distribution of radio emission for well known sources with quite regular structures can lead to values of  $a_0$  discrepant with those predicted by X-ray observations, the only presently available method to determine the source environment (cf. an extensive discussion of this problem in Kaiser 2000). In our statistical approach we assume  $a_0 = 10$  kpc for all sources, a conservative value between 2 kpc used by KDA and 50 kpc found by Wellman et al. (1997). In Section 5.1 we discuss the consequences of other possible values of this parameter.

We also use a constant value of  $\beta$  for all sample sources taking  $\beta = 1.5$  for further calculations. This is compatible with other estimates of this parameter (e.g. Daly 1995) although much flatter than  $\beta = 1.9$  adopted in the original KDA paper on the basis of Canizares et al.’s (1987) paper who found that value to be typical for a galaxy at about 100 kpc from its centre. A flatter density profile should be more adequate for distances of a few hundreds of kpc.

Another free parameter of the model, the orientation of the jet axis with respect to the observer’s line-of-sight  $\theta = 90^\circ$  is assumed for all *giants* and  $\theta = 70^\circ$  for other sources. This latter value is justified by the dominance of FRII-type radio galaxies in our sample. In view of the unified scheme for extragalactic radio sources, an average orientation angle  $\langle\theta_{\text{RG}}\rangle \simeq 69^\circ$  for radio galaxies only was determined by Barthel (1989). The apparent linear size  $D$  of a radio source then yields the model cocoon size:

$$L_j = \frac{D}{2 \sin \theta} \quad (9)$$

Having fixed all these free parameters of the model, we find the jet power  $Q_0$  and the initial density of external medium  $\rho_0$  for each individual sample source by iterative solution of the system of two equation: (i) equation (1) equated to equation (9) for the jet length  $L_j$ , and (ii) the integral for the luminosity of the cocoon  $P_v$  [equation (16) in KDA; cf. Section 3.1.2] – requiring the match of the solution to the observed values of  $D$  and  $P_{1.4}$ , respectively. The above fitting procedure proved to give always stable and unique solutions. Then, from equations (2) and (5) we calculate other model parameters: the cocoon’s pressure  $p_c$  and its energy density  $u_c$ , and from equation (7) the total cocoon energy  $E_{\text{tot}}$ . The resultant values of  $Q_0$ ,  $\rho_0$  and  $p_c$  for the sample sources are given in columns 6, 7, and 8 of Table 2.

In Table 3 we summarize meanings of the observational and model parameters characterizing the source’s cocoon and used in the present analysis. All dimensions are given in the SI units except the cocoons’ length and volume which are given in kpc and  $\text{kpc}^3$ , respectively. Two quantities present in the text do not appear in Table 3: the source (cocoon) unprojected linear size  $D_s$  and unprojected volume  $V_c$  which imply from the apparent (observed) size  $D$ , axial ratio  $AR$ , and assumed inclination of the sources’ axis  $\theta$ .

## 4 Results of the Modelling

### 4.1 Jet Power $Q_0$ and Core Density $\rho_0$

In the KDA model the jet power and ambient density are independent in accordance with a physical intuition. A distribution of these parameters derived for different sets of the sample sources on the  $\log(Q_0)$ – $\log(\rho_0)$  plane is shown in Figure 1a. One can realise in Figure 1a that *giants* are not fully separated from other sources, where (i) among the sources with a comparable jet power  $Q_0$ , *giant* sources have an average central density  $\rho_0$  smaller than a corresponding central density of normal-size sources, (ii) *giants* have at least ten times more powerful jets than much smaller low-luminosity sources of a comparable  $\rho_0$ .

Moreover, for a number of sources in the sample the derived values of their fundamental parameters  $Q_0$  and  $\rho_0$  are very close, while their ages are significantly different. Thus in view of the model assumptions, they may be considered as ‘the same’ source observed at different epochs of its lifetime. Such bunches of three to five sources (hereafter called ‘clans’) are indicated in Figure 1a with the large circles. These clans have appeared crucial in a comparison of the observing data and the model predictions, and in the analysis of the *giant*-source phenomenon. More detailed analysis of these clans and their evolution will be given in Paper II of this series.

The KDA and BWR models predict that the luminosities of mature radio sources decrease with their age. Therefore, more distant sources fall below the flux-density limit of a sample sooner than nearer sources, and in any sample the high-redshift sources will be younger and more luminous than the low-redshift ones. A significant anticorrelation between  $Q_0$  and age  $t$ , expected as a consequence of the above effect (called ‘youth-redshift degeneracy’ in BWR), is shown in Figure 1b.

### 4.2 Cocoon’s Energy Density $u_c$ and Total Emitted Energy $E_{\text{tot}}$

In the KDA model, the energetics of the radio source is governed by the jet power  $Q_0$ , adiabatic index  $\Gamma_c$ , and the pressure ratio  $\mathcal{P}_{\text{hc}}$ . Since  $\Gamma_c$  is assumed constant for all the sources and  $Q_0$  is constant for a given source, the energy of the cocoon  $u_c$  is determined by the pressure  $p_c$  attained by the cocoon at age  $t$ . As it decreases with time [cf. Equations (5), (3) and (2)] and the volume increases with time [Equation (6)], their product, i.e. the model total emitted energy,  $E_{\text{tot}}$ , is the increasing function of time, and its value is a fraction of energy delivered by the jet since the source’s birth,

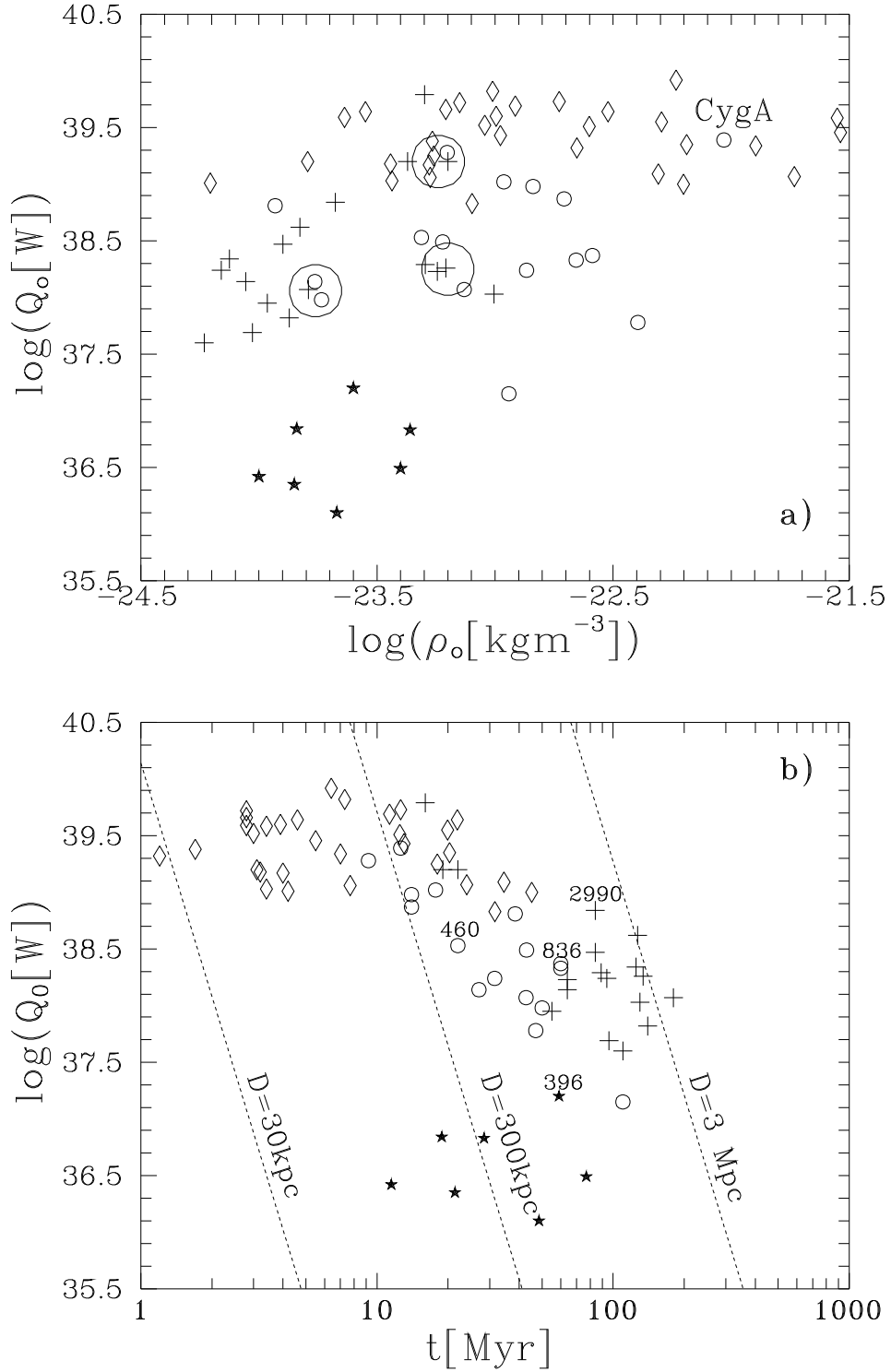


Figure 1: Plots of the jet power  $Q_0$  **a)** against central density of the core  $\rho_0$ ; **b)** against source age. The *giants* are indicated by crosses, high-redshift sources – diamonds, low-redshift sources – open circles, and low-luminosity sources – stars. The dotted lines mark a constant linear size predicted from equation (10). The numbers above some symbols indicate observed size of the marked source.

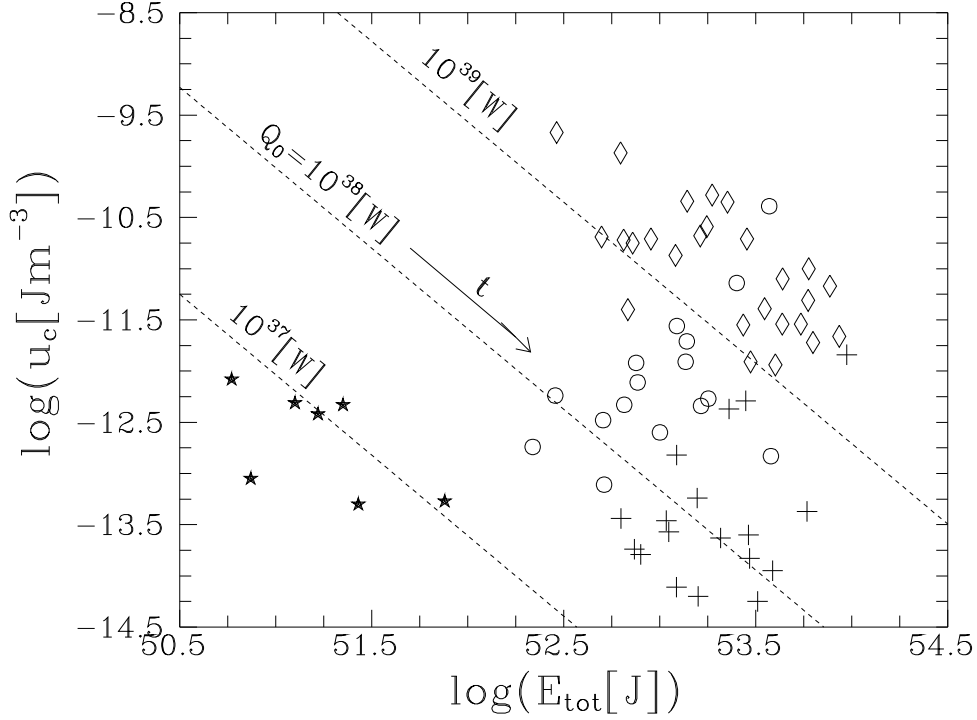


Figure 2: Plot of the energy density  $u_c$  against total emitted energy  $E_{\text{tot}}$ . The symbols indicating sources are the same as in Figure 1. Dotted lines mark the time axes for different values of  $Q_0$ .

$Q_0 t$  [cf. Equation (7)]. A distribution of  $u_c$  and  $E_{\text{tot}}$  parameters on the  $\log(u_c)$ – $\log(E_{\text{tot}})$  plane is shown in Figure 2. The time axes, calculated with Equations (2), (5) and (7) for a constant jet power, are indicated by the dotted lines.

In order to investigate the time evolution of *giant* radio sources on the basis of dynamical evolution of the entire FR II-type population, in the next Subsection we examine several correlations between the basic physical parameters of the sample sources derived from the data and the above two models. In the result we realize that all statistical tendencies are similar in both models. Therefore, below we present these correlations between parameters derived with the preferred KDA model only.

### 4.3 Correlations between Observed and Model Parameters

Below we analyse the relations between principal observational and model parameters of the sample sources important for their time evolution. Most of these parameters are interdependent (for example: the linear size of a source is likely dependent both on its age and the ambient medium density), hence each parameter of sources in our sample correlates somehow with other parameters. Therefore, in order to determine which correlation is the strongest,

we calculate the Pearson partial correlation coefficients between selected parameters. For the reason that most correlations between different parameters seem to be a power law, all correlations are calculated between logarithms of the given parameters (for the sake of simplicity, the ‘log’ signs are omitted in all Tables showing the partial correlations). Hereafter  $r_{XY}$  denotes the correlation coefficient between parameters  $X$  and  $Y$ ,  $r_{XY/W}$  is the partial correlation coefficient between these parameters in the presence of a third one, ( $W$ ), which can correlate with both  $X$  and  $Y$ , and  $P_{XY/W}$  is the probability that the test pair  $X$  and  $Y$  is uncorrelated when  $W$  is held constant. Similarly,  $r_{XY/VW}$ ,  $r_{XY/UVW}$ ,  $P_{XY/VW}$ , and  $P_{XY/UVW}$  are the correlation coefficients for the correlations involving four or five parameters, and the related probabilities, respectively.

A strong correlation between linear size and spectral age of 3C radio sources was already noted by Alexander and Leahy (1987) and confirmed by Liu et al. (1992). This correlation in our samples is shown in Figure 3. The giant sources do not show any tendency to a faster expansion velocity than that for the normal-size sources. The same conclusion has been made by Schoenmakers et al. (2000). However, two other aspects are worth emphasizing: (i) There are four high-redshift *giants* which are much younger than the low-redshift *giants*. Two of them are quasars. It seems that they might grow so large under some exceptional conditions. (ii) The  $D - t$  relation for the low-luminosity sources (mostly B2) follows the same slope of the correlation as that for other sources, but low-luminosity sources are definitely much smaller indicating a dependence of the size and expansion velocity on the source luminosity.

The partial correlation coefficients between the size  $D$  and  $t$ ,  $Q_0$ , and  $\rho_0$  together with the related probabilities of their chance correlation are given in Table 4.

In view of the dynamical model applied and as a result of the above statistical correlations, we see that the linear size of a source strongly depends on both its age and the jet power, where the correlation with age is the strongest. However, the size also anti-correlates with central density of the core. That anticorrelation seems to be a weaker than the correlations with  $Q_0$  and  $t$  and become well pronounced only when all three remaining parameters ( $Q_0$ ,  $t$  and  $z$ ) are kept constant.

Fitting a surface to the values of  $D$  over the  $t$ - $Q_0$  plane, we find

$$D(t, Q_0) \propto t^{1.06 \pm 0.03} Q_0^{0.31 \pm 0.02}. \quad (10)$$

The above relation well illustrates the influence of the jet power on the source (cocoon) expansion velocity, i.e. its length at a given age. However, the source expansion velocity ought to depend also on the external environment

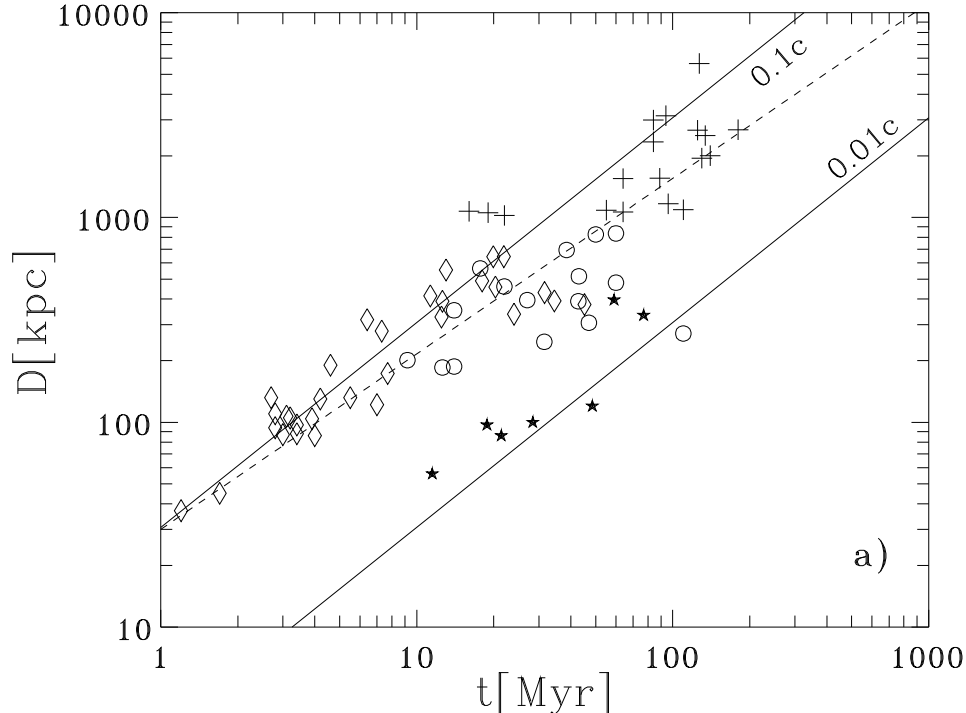


Figure 3: Plot of the linear size  $D$  against source age  $t$ . The symbols indicating sources are the same as in Figure 1. The solid lines indicate the implied expansion velocities in the speed of light  $c$  units. The dashed line shows the model predicted  $D(t) \propto L_j(t)$  relation resulting from Equation (1) for  $\beta=1.5$ .

conditions. Indeed, the significant partial correlation coefficient for the  $D-\rho_0$  correlation in Table 4 confirms this effect.

A greater than one exponent of the age in Equation (10) may suggest a statistical acceleration of the expansion velocities with age which contradicts with the deceleration implied by Equation (1) for  $\beta=1.5$  (shown with the dashed line in Figure 3). However, the observed luminosities of the sample sources demand different jet powers (cf. see below). A linear regression of their apparent  $D$  values transformed to a constant reference value of  $Q_0$  with Equation (10) on the age axis gives  $D(t) \propto t^{1.05 \pm 0.05}$ . This is somehow a surprised result and there would be several explanations of it: (i)  $\beta > 2$ , (ii) non-constant  $Q_0$  during the lifetime of sources, (iii) not representative sample of sources, or (iv) real possibility of an acceleration of the expansion speed, at least for sources evolving in a specific environmental conditions. We will return to this possibility in Paper II.

The partial correlation coefficients calculated for the correlation between the luminosity  $P_{1.4}$  and  $t$ ,  $Q_0$  and  $1+z$ , as well as the related probabilities of their chance correlations are given in Table 5.

Table 5 shows that the strongest correlation is between the source apparent luminosity and its jet power, although the anticorrelation between the luminosity and age is also significant. The model values of  $Q_0$  vs. the observed

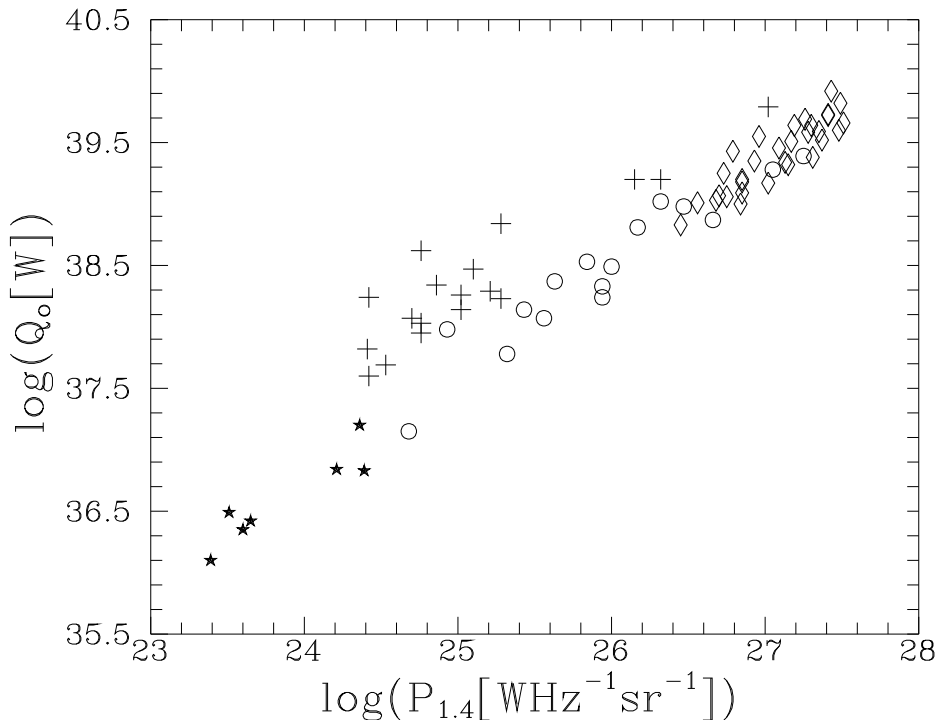


Figure 4: Plot of the model jet power  $Q_0$  against the observed 1.4 GHz luminosity of the sample sources.

1.4-GHz luminosities of the sample sources are plotted in Figure 4.

The *giant* sources seemingly have either a higher jet powers or lower radio luminosities than the normal-size sample sources. According to the model applied, the source luminosity (at a constant  $Q_0$ ) decreases with time, thus Figure 4 confirms that the *giants*, statistically older than normal-size sources in the sample (cf. Table 2), are less luminous than younger comparison sources with a similar  $Q_0$ .

Fitting a surface to the values of  $P_{1.4}$  over the  $t$ - $Q_0$  plane, we find

$$P_{1.4}(t, Q_0) \propto t^{-0.61 \pm 0.08} Q_0^{0.99 \pm 0.05}.$$

An anticorrelation between apparent luminosity and age of matured sources has been predicted by the KDA and BWR analytical models. The data of the sample sources allow to verify those predictions. This anticorrelation in our sample is shown in Figure 5 where the 1.4-GHz luminosities are transformed to the constant jet power of  $10^{38}$  W according to the surface fit given above. There is an evident lack of powerful old sources concordant with predictions of the above two models. However, the luminosity of *giant* sources seems to decrease faster with respect to that predicted by the KDA model and very likely is connected with a departure from the self-similarity of the cocoon expansion in that model. Therefore our data on *giant* sources support rather the evolutionary predictions of the BWR model.

The first time (to our knowledge) axial ratios of *giant* sources were analysed and compared with those of smaller FR II-type sources by Subrah-

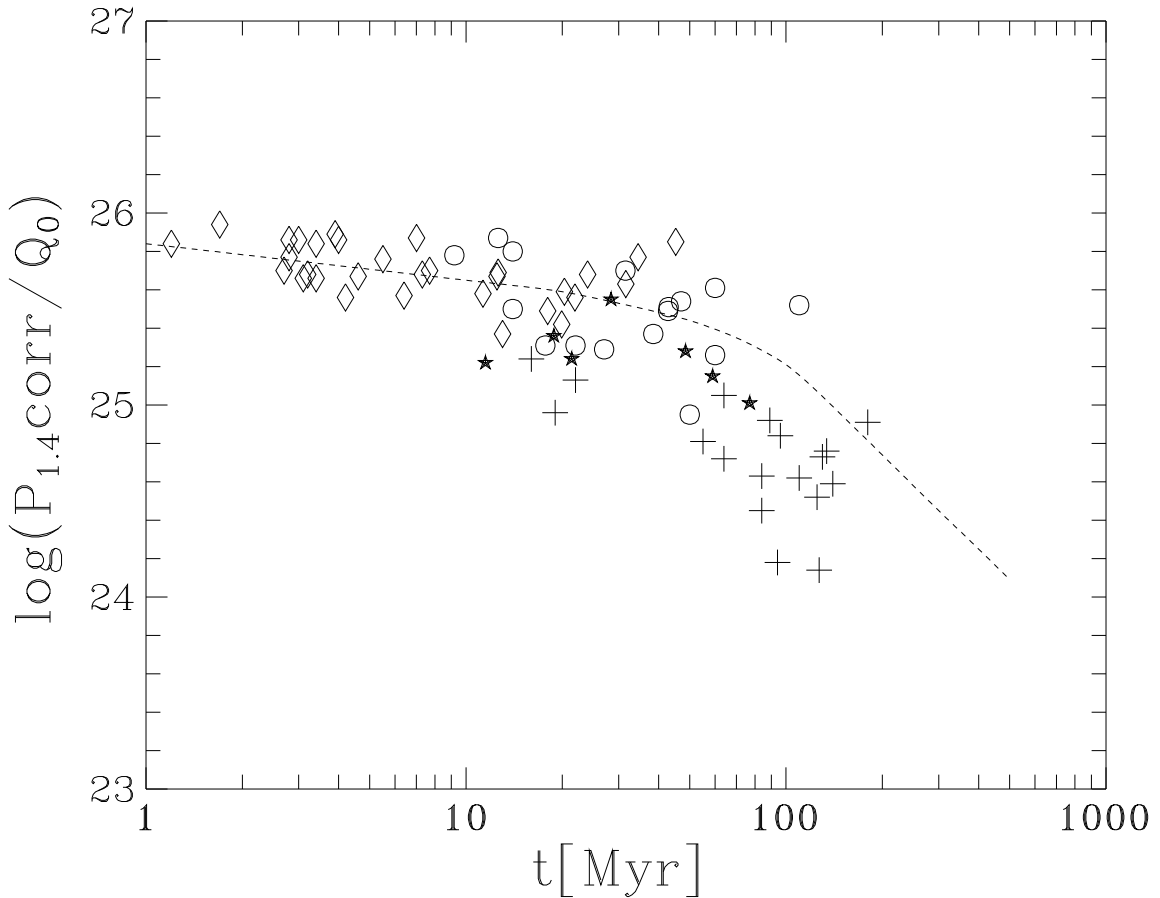


Figure 5: Plot of the 1.4 GHz luminosity  $P_{1.4}$  transformed to a constant jet power of  $10^{38}$  W against the source age  $t$ . The symbols indicating sources are the same as in Figure 1. The dashed curve shows the  $P - t$  relation for  $Q_0=10^{38}$  W resulting from the iterative solution of the relevant KDA equations; cf. Section 3.3.

manyan et al. (1996), who found no difference between the axial ratios of eight *giants* and eight 3C sources with a median size of about 400 kpc. The authors did not specify which 3C sources were considered, but since all *giant* and normal sources were of comparable powers and at comparable redshifts, we assume they might be of similar ages, so the dependence of  $AR$  on time could not be visible.

In the BRW model the axial ratio of an individual source steadily increases throughout its lifetime. Moreover, that model implies a dependence of the  $AR$  on the jet power  $Q_0$ . The latter dependence was probably reflected by an apparent correlation between  $AR$  and the 178-MHz luminosity of 3C sources noted by Leahy and Williams (1984). Taking into account the unavoidable anticorrelation between  $Q_0$  and age in any sample of sources (cf. Section 4.1), in Table 6 we have calculated the partial correlation coefficients and the related probabilities of chance correlations between  $AR$  and  $t$ ,  $AR$  and  $Q_0$ , and  $AR$  and  $\rho_0$  when relevant combinations of the parameters  $t$ ,  $Q_0$ ,  $\rho_0$ , and  $1+z$  are kept constant.

Table 6 shows statistically significant correlations between the axial ratio and the source's age, as well as the axial ratio and the jet power. Fitting a surface to the values of  $AR$  over the  $Q_0-t$  plane (where  $Q_0$  is in watts and  $t$

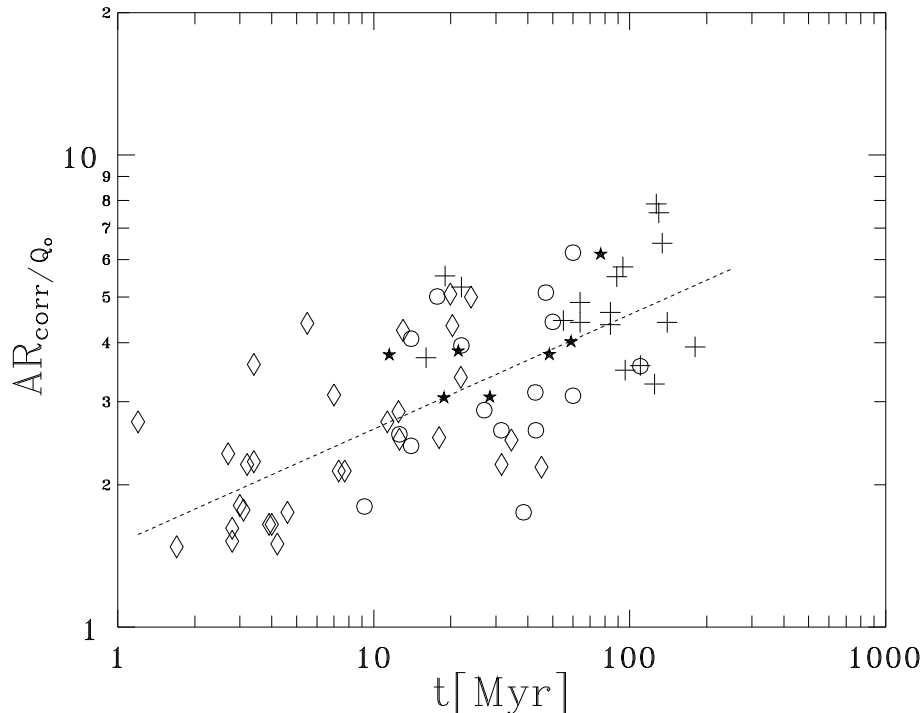


Figure 6: Plot of the source axial ratio transformed to a constant jet power of  $10^{39}$  W against the age  $t$ . The dashed line indicates the linear regression on the age axis.

in Myr), we found

$$AR(t, Q_0) \propto t^{0.23 \pm 0.03} Q_0^{0.12 \pm 0.02}. \quad (11)$$

Indeed, our statistical data strongly support the implication of the BRW model of the dependence of  $AR$  on  $Q_0$ . A consequence of this effect for the expansion speed of the cocoon is pointed out in the next subsection. Using the above relation, we transform the apparent  $AR$  values from Table 1 to a reference jet power of  $10^{39}$  W. The relation between the transformed axial ratio and age of the sample sources with the regression line on the time axis is shown in Figure 6.

This statistical correlation between the cocoon's axial ratio and age implies a time evolution of the ratio of the pressure in the head of the jet to the cocoon pressure. Indeed, substitution of Equation (11) into Equation (3) (for  $\beta=1.5$  with its assumed uncertainty of  $\pm 0.4$ ) gives:

$$\mathcal{P}_{hc}(t, Q_0) \propto t^{0.38 \pm 0.06} Q_0^{0.21 \pm 0.04}. \quad (12)$$

which violates the model assumption of self-similar expansion of the cocoon. The consequence of this will be analysed in Paper II.

Our statistical analysis confirms the significant anticorrelation between the cocoon pressure and the size of sources expected from Equation (2), but reveals also a significant correlation between this pressure and redshift.

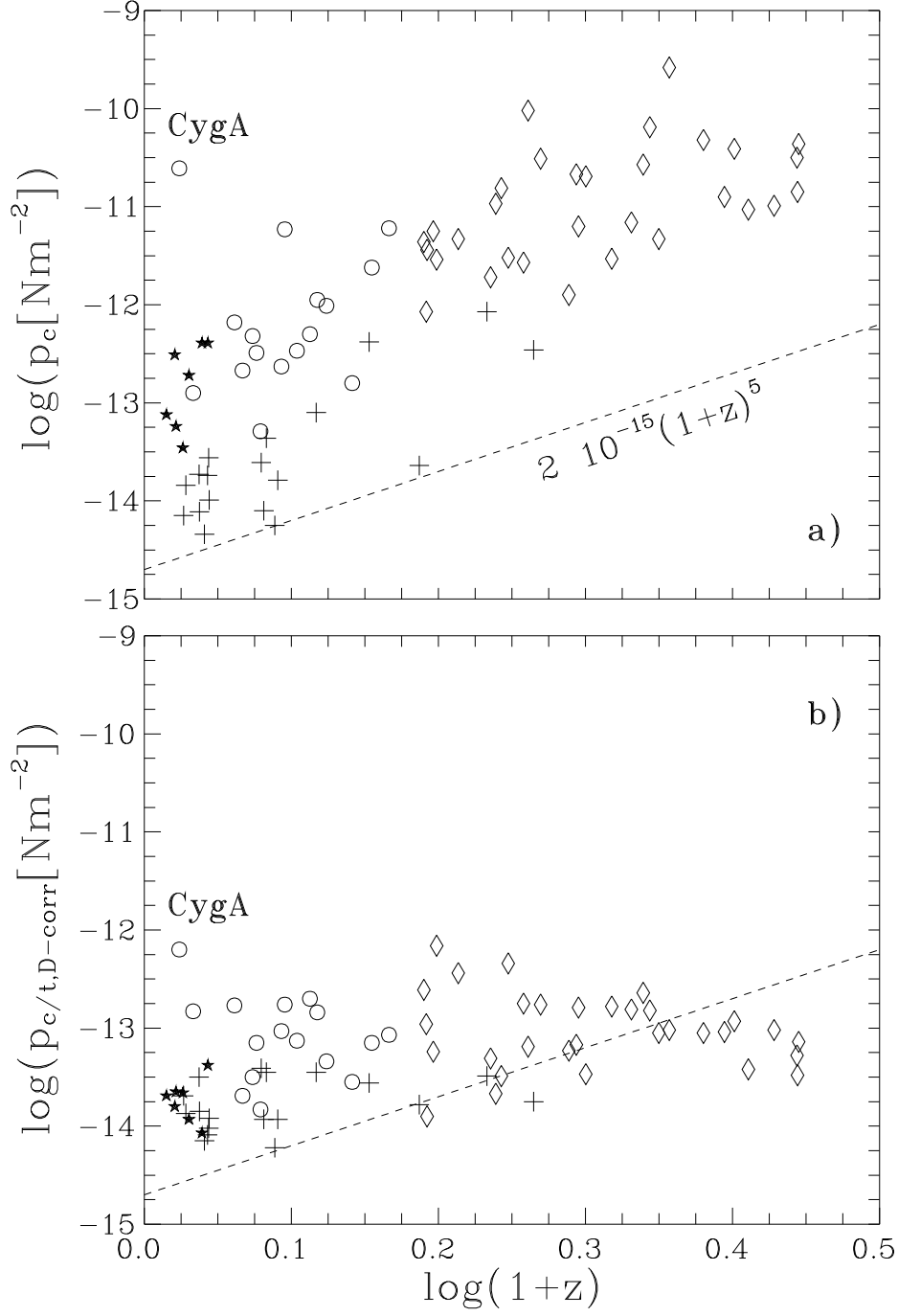


Figure 7: **a)** Cocoon pressure against size of the sample sources; **b)** the same pressure transformed to the reference size of 1 Mpc and age of 100 Myr against redshift. The symbols indicating sources within different sets are the same as in Figure 1 and 2. The dashed line in **a** and **b** indicates the presumed IGM pressure evolution  $p_{\text{IGM}} \propto (1+z)^5$ .

Besides, the size strongly correlates with age and anticorrelates with redshift, so we have calculated the partial correlation between all these parameters. The Pearson partial correlation coefficients between  $p_c$ ,  $D$ ,  $t$ , and  $1+z$  are given in Table 7.

Table 7 shows that: (i) The correlation coefficients for the direct ( $r_{XY}$ ) and partial ( $r_{XY/V}$ ,  $r_{XY/UV}$ ) correlations between the cocoon pressure and its size, and the cocoon pressure and the source age are very similar. This is obvious in view of the very high size–age correlation shown in Table 4. (ii) Both direct correlations are weakened, though still remain very significant, if the age and redshift (in the  $p_c - D$  correlation) and the size and redshift (in the  $p_c - t$  correlation) are kept constant. Formally, the strongest partial correlation is found between the cocoon pressure and size (in fact: the cocoon’s volume). (iii) the strong direct correlation between the cocoon pressure and redshift is seriously weakened if the source size and age are kept constant. This correlation, shown in Figure 7a, is very important for studies of physical conditions in the intergalactic medium (IGM). The dashed line indicates the expected electron pressure in an adiabatically expanding Universe in the form  $p_{\text{IGM}} = p_{\text{IGM}}^0(1+z)^5$  with  $p_{\text{IGM}}^0 = 2 \cdot 10^{-15} \text{ N m}^{-2}$  (cf. Subrahmanyam and Saripalli 1993).

Fitting a surface to the values of  $p_c$  over the  $D - t$  plane we find

$$p_c(D, t) \propto D^{-0.30 \pm 0.19} t^{-1.78 \pm 0.17}.$$

Therefore, one can transform the cocoon’s pressure values to a reference size and age. The plot of cocoon pressures transformed to  $D=1$  Mpc and  $t=100$  Myr versus  $1+z$  is shown in Figure 7b. This Figure illustrate how  $p_c$  of the high-redshift sources would decrease if they had evolved into the above size and age, and emphasize that the strong direct  $p_c - (1+z)$  correlation in Figure 7a is, in fact, due to the much stronger correlations  $p_c - D$  and  $p_c - t$  (cf. Table 7). However, this is purely statistical result and the question about conditions under which distant radio sources would reach very large size and old age remains open. The aspect of a cosmological evolution of the IGM is discussed in Section 5.4.

## 5 Discussion of the Results

### 5.1 Influence of Fixed Model Parameters on the Model Predictions

The basic physical parameters of the radio sources derived in this paper with the aim of the KDA model, i.e. jet power  $Q_0$ , central density  $\rho_0$ , and

cocoon pressure  $p_c$ , are in principle dependent on the assumed central core radius, the exponent in the external gas distribution, the adiabatic indices of electrons and magnetic field, as well as on the orientation of the jet axis towards the observer. In application of the KDA model we have assumed the same values of these parameters for all sample sources. This assumption can only be valid in our statistical analysis of the evolutionary trends in the whole FRII-type population but not for individual sample sources. In particular, we have adopted  $a_0 = 10$  kpc and  $\beta = 1.5$ , respectively. Taking a lower core radius, e.g.  $a_0 = 2$  kpc, and keeping  $\beta = 1.5$  will result in increase of the model density of the core  $\rho_0$  by roughly one order of magnitude, while other model parameters will not be changed. Conversely, a lower density gradient, e.g.  $\beta = 1.1$ , will lower  $\rho_0$  approximately  $1.5 \sim 6$  times. In this case however, the jet power will be increased by a few percent and accordingly the pressure and energy density in the cocoon will be changed. Solving the equations in Section 3 for a few sets of the model free parameters ( $a_0, \beta, \theta$ ) we find that the presented and discussed correlations between the observational and model parameters are not changed; all the statistical trends are preserved although the values of the model parameters (especially  $\rho_0$ ) are changed quantitatively.

A relativistic equation of state for the magnetic field does not change our results significantly, unless the KDA ‘Case 1’ ( $\Gamma_c = \Gamma_B = 4/3$ ) is adopted. However, this case, i.e. when both the cocoon and the magnetic field energy have a relativistic equation of state, is unlikely for our sample sources. Therefore, we argue that the results discussed below are not significantly biased by selection of a particular set of the model parameters.

## 5.2 Cause of Extremal Linear Size

In view of the KDA and BRW analytical models of dynamical evolution of FRII-type radio sources, many such sources can evolve into a stage characterized by a linear size exceeding 1 Mpc. Access to this stage depends on a number of the model parameters: jet power  $Q_0$ , its Lorentz factor  $\gamma_{\text{jet}}$ , the adiabatic indices of the cocoon material and magnetic field,  $\Gamma_c$  and  $\Gamma_B$ , respectively, as well as the core radius  $a_0$ , the external gas density  $\rho_0$ , and the exponent of its distribution  $\beta$ . For a given set of these parameters, the model allows us to determine whether an evolving source will reach the size of 1 Mpc, and if so, at what age. From this point of view, *giant* sources should be the oldest ones.

In this paper (Section 4.3) we have confronted the KDA model predictions with the observational data on *giant*-size and normal-size FRII sources. Our statistical analysis strongly suggests that there is not a single evolutionary

scheme governing the size development. An old age or a low external density alone is insufficient to assure extremely large linear extent of a source, both are necessary together with a suitable power driven from AGN by the highly relativistic jets. The Pearson partial correlation analysis indicates that the dependence of linear size on each of these three parameters is statistically significant. Ordering these correlations by decreasing partial correlation coefficients, we find that the size is dependent on age, then on  $Q_0$ ; next on  $\rho_0$ .

About 83 % of *giants* in our sample possess a projected linear size over 1 Mpc owing to statistically old age, low or moderate density of the external medium, and high enough power of their jets. The remaining 17 % (3 sources) are high luminosity sources at redshifts  $z > 0.4 \sim 0.5$  and ages from 15 to 25 Myr which are typical for normal-size sources. Two of them are quasars. The jet power of these sources is high enough to compensate for a higher ram pressure in a denser surrounding environment and higher energy losses during the cocoon expansion. The jet power of *giants* is not extreme, so several FR II-type sources having that  $Q_0$  can potentially achieve very large size after a suitably long time. According to our results (cf. Figure 1a), these potential *giants* should have  $Q_0 > 10^{37.5}$  W and be situated in an environment with  $\rho_0 < 10^{-23}$  kg m<sup>-3</sup>.

The above scenario is not caused by a selection effect. We show that there are low-luminosity sources which lie in the parts of  $\log Q_0 - \log \rho_0$  plane (Figure 1a) completely avoided by *giant* sources. They diverge from *giants* and even normal-size powerful sources by having low jet power  $Q_0 < 10^{37.5}$  W and total energy  $E_{\text{tot}} < 10^{52.5}$  J. Thus we suggest that they never reach the giant size. It is worth noting that some of them already have an age comparable to that of typical *giants*, in accordance with the model expectations.

### 5.3 Jet Power and Energy Budget

The ratio of total energy supplied by the twin jets during the lifetime of a source ( $2Q_0t$ ) and its energy stored in the cocoon, derived from the data under the assumption of energy equipartition,  $U_{\text{eq}} = u_{\text{eq}}V_0$ , allow another test of the dynamical model predictions. The ratio of  $2Q_0t/U_{\text{eq}}$  for the sample sources (given in column 9 of Table 2) is plotted in Figure 8 vs. the cocoon axial ratio  $AR$ . The uncertainties in both values are marked by error bars on some data points. The solid curve indicates the model prediction from Equation (8), while the dashed curve shows the best fit to the data. The observed trend fully corresponds to the model prediction. However, the derived values of  $2Q_0t/U_{\text{eq}}$ , i.e. the reciprocal of the efficiency factor by which

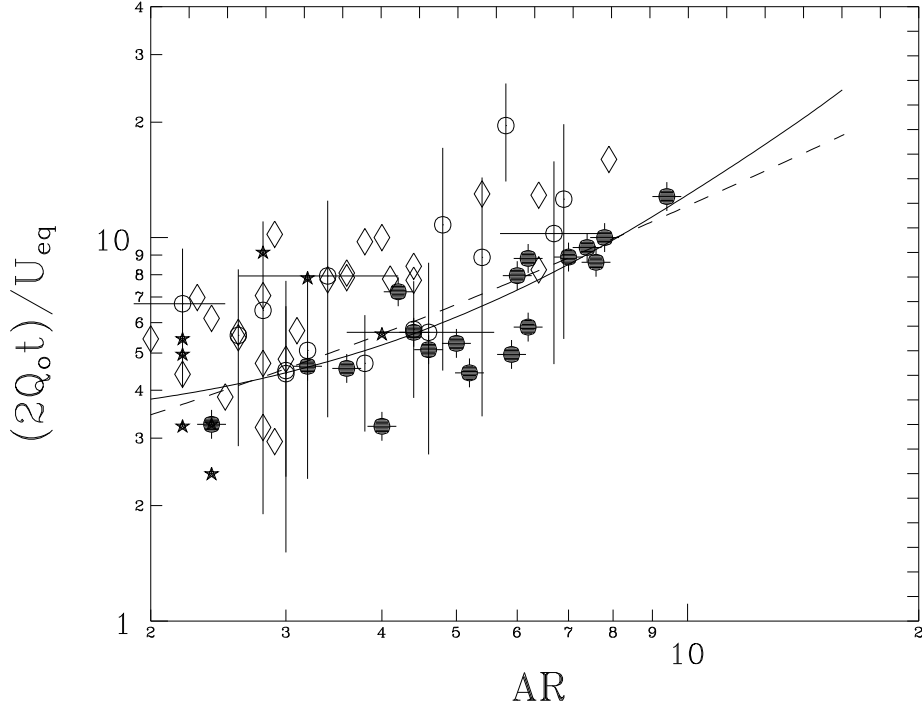


Figure 8: Ratio of the total energy supplied by twin jets and energy stored in the cocoon against its axial ratio  $AR$ . The large uncertainties in both parameters are marked by error bars for a few sources only for clarity. Here the giant sources are marked with filled circles. The solid curve indicates the model prediction from Equation (8); the dashed curve shows the best fit to the weighted data.

the kinematic energy of the jets is converted into radiation, is much higher than  $\sim 2$ , a value usually assumed in a number of papers.

In a number of studies of *giant* radio sources (e.g. Parma et al. 1996; Schoenmakers et al. 1998) the authors followed the approach of Rawlings and Saunders (1991) and assumed a fraction of the total jet energy wasted for adiabatic expansion of the cocoon to be about 0.5 and used it to estimate the jet power  $Q_0$  for sources with known age (almost always from spectral ageing analysis). In the KDA model the energy stored in the source (cocoon) is

$$E_{\text{tot}} \approx \int \{Q_0 dt - (p_c d[V_c(t)] + p_h d[V_h(t)])\}$$

where  $p_c dV_c + p_h dV_h$  is the work done to expand the cocoon, and  $p_h$  and  $V_h$  are the hotspot pressure and volume, respectively. If  $V_h$  is neglected, the expansion work will be  $\approx 0.5 Q_0 t$ ; if not, it is dependent on the pressure ratio  $\mathcal{P}_{\text{hc}}$  as shown in Section 3.2.

The values of  $2Q_0 t/U_{\text{eq}}$  in our sample (Figure 8; Table 2) vary from about 2 to more than 10 due to the high jet power required for the adiabatic expansion of the cocoon. The  $Q_0$  values derived here from the KDA model can

be compared with the relevant values estimated by Wan, Daly and Guerra (2000) [WDG] for 22 3C sources included also in our sample (21 with  $z > 0.5$  + Cyg A). Recalculating their values for  $H_0 = 50 \text{ km s}^{-1} \text{ Mpc}^{-1}$  we found the WDG estimates approximately 2.5 times lower than the KDA values. Exactly the similar ratio ( $1.7 \div 5.5$  depending on the value of  $\mathcal{P}_{\text{hc}}$ ) characterize the jet powers of 9 3C sources, common with our sample sources, determined by Rawlings and Saunders (1991). The explanation of this ratio is straightforward. The values of  $Q_0$  estimated in those papers were based on the ram pressure considerations in the overpressured source model A of Scheuer (1974) and its further modifications (e.g. Begelman and Cioffi 1989; Loken et al. 1992; Nath 1995). They all are self-similar models of the Carvalho and O’Dea type I which describe the source dynamics only. If the source energetics and especially the energy losses are properly taken into account (the type III models; e.g. KDA, BRW), the significantly higher values of  $Q_0$  are implied.

The data in our sample show a dependence of the energy ratio  $2Q_0 t / U_{\text{eq}}$  on the cocoon axial ratio  $AR$ , and imply an increase of the fraction of jet energy spent on the adiabatic expansion of the cocoon volume in time. However, the data also suggest that for a constant  $AR$  (i.e. a given geometry of the cocoon), *giants* tend to have a smaller ratio of  $2Q_0 t / U_{\text{eq}}$  than normal-size sources which means less energy of the jets converted into adiabatic expansion of the cocoon. This may indicate a lower pressure of the external medium surrounding the *giant* sources than that around smaller ones.

## 5.4 External Pressure of the Surrounding Medium and its Evolution

A non-relativistic uniform intergalactic medium (IGM) in thermal equilibrium filling an adiabatically expanding Universe should have an electron pressure evolving with redshift  $p_{\text{IGM}} = p_{\text{IGM}}^0 (1 + z)^5$ . The advancing hotspots of FR II-type radio sources are probably confined by ram pressure of the IGM. *Giant* sources, with their lobes extended far outside typical galaxy halo, have the lowest values of  $p_c$  and may be useful for determining the upper limit of  $p_{\text{IGM}}$ . Using a small sample of *giant* sources, Subrahmanyan and Saripalli (1993) limited its local value to  $p_{\text{IGM}}^0 \approx (0.5 \div 2) \cdot 10^{-15} \text{ N m}^{-2}$ . A further study was undertaken by Cotter (1998) who, using a larger sample of 7C giants with sources out to redshift of  $\sim 0.9$ , confirmed a strong dependence of the lowest  $p_c$  on redshift in agreement with a  $(1 + z)^5$  relation. This observational result has been critically discussed by Schoenmakers et al. (2000), who have considered possible selection effects in Cotter’s analysis (including the Malmquist bias), and concluded that there was not evidence in their

own sample for a cosmological evolution of  $p_{\text{IGM}}$ . However, they also state that this hypothesis cannot be rejected until some low-pressure high-redshift sources are found.

In all the above analyses the age of sources was not considered. The very significant correlation between  $p_c$  and  $D$  or  $t$ , shown in Section 4.3, strongly suggests that the intrinsic dependences of size on age as well as of age on redshift and not the Malmquist bias is mainly responsible for the apparent correlation between  $p_c$  and  $1+z$ . Nevertheless, we agree with Schoenmakers et al.’s conclusion that until *giant* sources with internal pressures in their lobes  $p_c < 2 \cdot 10^{-15} \text{ N m}^{-2}$  at redshifts of at least  $0.6 \div 0.8$  are not discovered, the IGM pressure evolution in the form  $p_{\text{IGM}} \propto (1+z)^5$  cannot be rejected.

Most *giants* in our sample, except four high-redshift ones, reveal the lowest pressure in their cocoons. Sharing Subrahmanyam and Saripalli’s arguments, we can expect those cocoon pressures are indicative of an upper limit to the present-day external pressure of the IGM,  $p_{\text{IGM}}^0$ . Taking into account the lowest values of  $p_c$  (cf. Figure 7a), we found  $p_{\text{IGM}}^0 < 2 \cdot 10^{-15} \text{ N m}^{-2}$  in accordance with their value. It is worth emphasizing that the above results are obtained from the analytical model assuming energy equipartition in the initial ratio of the energy densities of the magnetic field and the particles (cf. Section 3.1). This may not be the case in every part of the source (cocoon). Hardcastle and Worrall (2000) estimated gas pressures in the X-ray-emitting medium around normal-size 3CRR FR II radio galaxies and quasars, and found that, with few exceptions, the minimum pressures in their lobes, determined under equipartition conditions, were well below the environment pressures measured from old ROSAT observations. Therefore, they have argued that there must be an additional contribution to the internal pressure in lobes of those sources likely including pressure from protons, magnetic fields exceeding their minimum-energy values, or non-uniform filling factors. Nevertheless, the diffuse lobes of *giants*, extending farther from a host galaxy than the typical radius of high-density X-ray-emitting gas, may be in equilibrium with an ambient medium the emissivity of which is not directly detectable.

## 6 Conclusions

In this paper we confront the analytical KDA model predictions with the observational data of ‘giant’ and normal size FR II-type radio sources. From our analysis we can conclude as follows:

- (1) *Giant* sources do not form a separate class of radio sources, and do not reach their extremal sizes exclusively due to some exceptional physical

conditions of the external medium. The size is dependent, in order of decreasing partial correlation coefficients, on age; then on the jet power  $Q_0$ ; next on the central core density  $\rho_0$ .

(2) *Giants* possess the lowest equipartition magnetic field strength and energy density of their cocoons making their detection difficult in synchrotron emission. However, their accumulated total energy is the highest among all sources and exceeds  $3 \cdot 10^{52}$  W.

(3) Our data confirm the conclusion drawn by Blundell et al. (1999) that throughout the lifetime of an individual source its axial ratio can steadily increase, thus its expansion cannot be self-similar all the time. A self-similar expansion seems to be feasible if the power supplied by the jets is a few orders of magnitude above the minimum-energy value. In other cases the expansion can only initially be self-similar; a departure from self-similarity for large and old sources is justified by observations of *giant* sources.

(4) The apparent increase of the lowest cocoon pressures (observed in the largest sources) with redshift is mainly caused by the intrinsic dependence of their age on redshift and dominates over a bias by possible selection effects. However, a cosmological evolution of the IGM cannot be rejected until *giant* sources with internal pressures in their lobes less than  $2 \cdot 10^{-15}$  N m<sup>2</sup> at high redshifts are *not* discovered.

## 7 Acknowledgements

We thank Dr. C. R. Kaiser for explanations of the integration procedures used in the KDA paper.

## References

- Alexander, P., and Leahy J.P. 1987, *MNRAS*, 225, 1  
Barthel, P.D. 1989, *ApJ*, 336, 606  
Becker, R.H., White, R.L., and Helfand, D.J. 1995, *ApJ*, 450, 559  
Begelman, M.C., and Cioffi, D.F. 1989, *ApJ*, 345, L21  
Blundell, K.M., Rawlings, S., and Willott, C.J. 1999, *AJ*, 117, 766  
Canizares, C.R., Fabbiano, G., and Trinchieri, G. 1987, *ApJ*, 312, 503  
Carilli, C.L., Perley, R.A., Dreher, J.W., and Leahy, J.P. 1991, *ApJ*, 383, 554  
Carvalho, J.C., and O’Dea, C.P. 2002, *ApJS*, 141, 337  
Condon, J.J., Cotton, W.D., Greisen, E.W., Yin, Q.F., Perley, R.A., Taylor, G.B., and Broderick, J.J. 1998, *AJ*, 115, 1693  
Cotter, G., 1998 “Observational cosmology with the new sky surveys” Eds.: M.N. Bremer et al. (Kluwer Acad. Publ.), p.233

Daly, R.A. 1995, *ApJ*, 454, 580  
 de Ruiter, H.R., Parma, P., Fanti, C., and Fanti, R. 1986, *A&AS*, 65, 111  
 Fanaroff, B.L., and Riley, J.M. 1974, *MNRAS*, 167, 31P  
 Fanti, C., Fanti, R., de Ruiter, H.R., and Parma, P. 1986, *A&A*, 65, 145  
 Guerra, E.J., Daly, R.A., and Wan, L. 2000, *ApJ*, 544, 659  
 Hardcastle, M.J., and Worrall, D.M. 2000, *MNRAS*, 319, 562  
 Hine, R.G. 1979, *MNRAS*, 189, 527  
 Ishwara-Chandra, C.H., and Saikia, D.J. 1999, *MNRAS*, 309, 100  
 Jaffe, W.J., and Perola, G.C. 1973, *A&A*, 26, 423  
 Kaiser, C.R. 2000, *A&A*, 362, 447  
 Kaiser, C.R., and Alexander, P. (KA) 1997, *MNRAS*, 286, 215  
 Kaiser, C.R., and Alexander, P. 1999, *MNRAS*, 302, 515  
 Kaiser, C.R., Dennett-Thorpe, J., and Alexander, P. (KDA) 1997, *MNRAS*, 292, 723  
 King, I.R. 1972, *ApJ*, 174, L123  
 Klein, U., Mack, K.-H., Gregorini, L., and Parma, P. 1995, *A&A*, 303, 427  
 Lara, L., Mack, K.-H., Lacy, M., Klein, U., Cotton, W.D., Feretti, L., Giovannini, G., and Murgia, M. 2000, *A&A*, 356, 63  
 Loken, C., Burns, J.O., Clarke, D.A., and Norman, M.L. 1992, *ApJ*, 392, 54  
 Leahy, J.P., Muxlow, T.W.B., and Stephens, P.W. 1989, *MNRAS*, 239, 401  
 Leahy, J.P., and Williams, A.G. 1984, *MNRAS*, 210, 929  
 Liu, R., Pooley, G., and Riley, J.M. 1992, *MNRAS*, 257, 545  
 Machalski, J., and Condon, J.J. 1983, *AJ*, 88, 1591  
 Machalski, J., and Condon, J.J. 1985, *AJ*, 90, 5  
 Machalski, J., and Jamrozy, M. 2000, *A&A*, 363, L17  
 Machalski, J., Jamrozy, M., and Zola, S. 2001, *A&A*, 371, 445  
 Mack, K.-H., Klein, U., O'Dea, C.P., and Willis, A.G. 1997, *A&AS*, 123, 463  
 Mack, K.-H., Klein, U., O'Dea, C.P., Willis, A.G., and Saripalli, L. 1998, *A&A*, 329, 431  
 Miley, G.K. 1980, *ARA&A*, 18, 165  
 Myers, S.T., and Spangler, S.R. 1985, *ApJ*, 291, 52  
 Nath, B.B. 1995, *MNRAS*, 274, 208  
 Parma, P., de Ruiter, H.R., Fanti, C., and Fanti, R. 1986, *A&AS*, 64, 135  
 Parma, P., de Ruiter, H.R., Mack, K.-H., van Breugel, W., Dey, A., Fanti, R., and Klein, U. 1996, *A&A*, 311, 49  
 Parma, P., Murgia, M., Morganti, R., Capetti, A., de Ruiter, H.R., and Fanti, R. 1999, *A&A*, 344, 7  
 Rawlings, S., and Saunders, R. 1991, *Nature*, 349, 138  
 Saripalli, L., Subrahmanyan, R., and Hundstead, R.W. 1994, *MNRAS*, 269, 37  
 Scheuer, P.A.G. 1974, *MNRAS*, 166, 513

- Schoenmakers, A.P., de Bruyn, A.G., Röttgering, H.J.A., and van der Laan, H. 2001, *A&A*, 374, 861
- Schoenmakers, A.P., Mack, K.-H., Lara, L., Röttgering, H.J.A., de Bruyn, A.G., van der Laan, H., and Giovannini, G. 1998, *A&A*, 336, 455
- Schoenmakers, A.P., Mack, K.-H., de Bruyn, A.G., Röttgering, H.J.A., Klein, U., and van der Laan, H. 2000, *A&AS*, 146, 293
- Spangler, S.R., and Pogge, J.J. 1984, *AJ*, 89, 342
- Subrahmanyam, R., and Saripalli, L. 1993, *MNRAS*, 260, 908
- Subrahmanyam, R., Saripalli, L., and Hundstead, R.W. 1996, *MNRAS*, 279, 257
- Urry, C.M., and Padovani, P. 1995, *PASP*, 107, 803
- Wan, L., Daly, R.A., and Guerra, E.J. 2000, *ApJ*, 544, 671
- Wellman, G.F., Daly, R.A., and Wan, L. 1997, *ApJ*, 480, 96

## Observational data and physical parameters of the sample sources

Table 1 gives the observational data of the sample sources. Their radio luminosity, size and volume are calculated with  $H_0=50 \text{ km s}^{-1}\text{Mpc}^{-1}$  and  $q_0=0.5$ . The entries are:

*Column 1:* IAU-format name of source

*Column 2:* Other name

*Column 3:* Redshift

*Column 4:* Logarithm of 1.4 GHz luminosity

*Column 5:* Projected linear size

*Column 6:* Source axial ratio

*Column 7:* Logarithm of source volume

*Column 8 and 9:* References to the radio maps and spectral ageing analysis, respectively

Table 2 contains the adopted age and physical parameters of the sample sources derived either from the observational data (columns 3, 4, and 5) and from the analytical KDA model (columns 6, 7, 8, and 9). The entries are:

*Column 2:* Age of source

*Column 3:* Logarithm of the equipartition energy density

*Column 4:* Equipartition magnetic field strength

*Column 5:* Logarithm of the source total energy

*Column 6:* Logarithm of the jet power

*Column 7:* Logarithm of the initial density of the external medium at the core radius  $a_0$

*Column 8:* Logarithm of the cocoon pressure

*Column 9:* Ratio between the total energy of twin jets and the source energy.

Table 1: Data of the sample sources

IAU name	Other name	$z$	$\lg P_{1.4}$ [WHz <sup>-1</sup> sr <sup>-1</sup> ]	$D \pm \Delta D$ [kpc]	AR $\pm\Delta$ AR	$\lg V_o \pm \Delta \lg V_o$ [kpc <sup>3</sup> ]	Ref. map	Spect. anal.
GIANTS								
0109+492	3C35	0.0670	24.53	1166±31	3.2±0.7	8.08±0.17	28	24
0136+396	B2	0.2107	25.21	1555±35	6.0±1.2	7.91±0.16	4	6
0313+683	WNB	0.0901	24.41	2005±34	4.2±0.5	8.55±0.10	28	23
0319-454	PKS	0.0633	24.70	2680±30	4.0±0.8	8.98±0.16	22	22
0437-244	MRC	0.84	26.15	1055±17	7.8±1.5	7.18±0.15	5	5
0813+758	WNB	0.2324	25.10	2340±80	5.0±0.5	8.60±0.08	25	24
0821+695	8C	0.538	25.28	2990±22	5.9±1.0	8.77±0.14	7	7
1003+351	3C236	0.0988	24.76	5650±75	9.4±1.7	9.20±0.14	15	16
1025-229	MRC	0.309	25.28	1064±17	5.2±0.7	7.54±0.11	5	5
1209+745	4C74.17	0.107	24.42	1090±13	2.4±0.5	8.25±0.16	2	24
1232+216	3C274.1	0.422	26.32	1024±15	7.4±1.6	7.19±0.17	8	1
1312+698	DA340	0.106	24.76	1085±12	4.4±0.9	7.71±0.16	28	24
1343+379		0.2267	24.42	3140±60	7.2±1.1	8.67±0.14	28,14	13
1349+647	3C292	0.71	27.02	1073±16	6.2±1.4	7.40±0.18	28	1
1358+305	B2	0.206	24.86	2670±60	3.6±0.8	9.06±0.17	19	19
1543+845	WNB	0.201	24.76	1950±25	7.6±1.4	8.00±0.15	28	24
1550+202	3C326	0.0895	25.02	2510±55	7.0±1.1	8.40±0.13	28	16
2043+749	4C74.26	0.104	24.86	1550±20	4.6±0.8	8.14±0.14	28	24
NORMAL								
0154+286	3C55	0.720	26.79	554±12	6.4±1.5	6.54±0.18	9	9
0229+341	3C68.1	1.238	27.26	414±10	4.4±1.0	6.49±0.18	9	9
0231+313	3C68.2	1.575	27.30	190±4	2.8±0.6	5.86±0.14	9	9
0404+428	3C103	0.330	26.32	564±12	6.7±1.0	6.53±0.12	8	1
0610+260	3C154	0.5804	26.84	376±10	2.9±0.8	6.72±0.21	9	9
0640+233	3C165	0.296	25.94	480±8	3.4±0.8	6.90±0.18	8	1
0642+214	3C166	0.246	26.66	187±15	3.1±0.6	5.76±0.15	8	1,29
0710+118	3C175	0.768	26.85	392±8	3.4±0.9	6.64±0.20	9	9
0806+426	3C194	1.184	27.13	122±3	3.1±0.5	5.18±0.17	30	30
0828+324	B2	0.0507	24.36	396±14	3.2±0.4	6.71±0.10	12	6,20
0908+376	B2	0.1047	24.39	100±8	2.2±0.2	5.24±0.08	18	20
0958+290	3C234	0.1848	25.84	460±8	4.6±1.0	6.59±0.17	8	1
1008+467	3C239	1.786	27.51	94±3	2.6±0.7	5.01±0.21	10	10
1012+488	GB/GB2	0.385	26.17	694±13	2.2±0.3	7.76±0.11	12	29
1030+585	3C244.1	0.428	26.47	352±7	5.4±1.3	6.10±0.19	8	1
1056+432	3C247	0.749	26.85	105±4	3.1±0.7	5.00±0.18	10	10
1100+772	3C249.1	0.311	25.94	247±24	2.8±1.0	6.21±0.26	9	9
1111+408	3C254	0.734	26.85	107±4	2.5±0.3	5.22±0.10	10	10
1113+295	B2	0.0489	24.21	97±5	2.2±0.3	5.20±0.11	18	20
1140+223	3C263.1	0.824	27.31	45±5	2.2±0.4	4.20±0.14	10	10
1141+354	GB/GB2	1.781	26.68	97±3	3.0±0.4	4.93±0.11	11	29
1142+318	3C265	0.8108	27.19	644±16	5.4±1.7	6.89±0.24	9	1,9
1143+500	3C266	1.275	27.15	37±2	4.0±0.4	3.42±0.08	10	10

IAU name	Other name	$z$	$\lg P_{1.4}$ [ $\text{WHz}^{-1}\text{sr}^{-1}$ ]	$D \pm \Delta D$ [kpc]	$\text{AR} \pm \Delta \text{AR}$	$\lg V_o \pm \Delta \lg V_o$ [ $\text{kpc}^3$ ]	Ref. map	Spect. anal.
1147+130	3C267	1.144	27.17	327±8	4.4±0.7	6.18±0.13	9	9
1157+732	3C268.1	0.974	27.41	390±7	4.1±0.6	6.47±0.12	9	9
1206+439	3C268.4	1.400	27.37	87±4	2.8±0.3	4.85±0.09	10	10
1216+507	GB/GB2	0.1995	24.93	826±8	4.4±0.6	7.39±0.11	12	29
1218+339	3C270.1	1.519	27.48	104±12	2.6±0.5	5.15±0.15	10	10
1221+423	3C272	0.944	26.73	490±13	3.6±1.1	6.88±0.23	28	29
1241+166	3C275.1	0.557	26.56	130±15	2.0±0.4	5.66±0.16	10	10
1254+476	3C280	0.996	27.35	110±13	2.4±0.3	5.29±0.10	10	10
1308+277	3C284	0.2394	25.63	836±6	6.9±1.3	7.01±0.15	8	1
1319+428	3C285	0.0794	24.68	271±4	2.8±0.6	6.33±0.17	8	1
1343+500	3C289	0.967	27.02	86±2	2.3±0.2	5.00±0.07	10	10
1347+285	B2	0.0724	23.60	86±4	2.4±0.3	4.94±0.10	18	20
1404+344	3C294	1.779	27.41	132±17	3.8±1.0	5.12±0.20	10	10
1420+198	3C300	0.270	26.00	516±6	3.0±1.2	7.11±0.29	8	1
1441+262	B2	0.0621	23.51	333±8	4.0±0.9	6.28±0.18	21	20
1522+546	3C319	0.192	25.56	390±15	3.2±0.7	6.69±0.17	8	1
1533+557	3C322	1.681	27.49	279±7	3.6±0.7	6.15±0.15	9	9
1547+215	3C324	1.207	27.28	88±3	3.6±0.9	4.60±0.30	30	30
1549+628	3C325	0.860	27.09	132±4	4.4±0.9	4.97±0.28	30	30
1609+660	3C330	0.549	26.93	458±8	6.4±1.2	6.29±0.15	9	9
1609+312	B2	0.0944	23.65	56±4	2.4±0.3	4.41±0.10	3	20
1615+324	3C332	0.1515	25.32	306±7	4.8±1.3	6.02±0.21	3	20
1618+177	3C334	0.555	26.45	430±15	2.8±0.4	6.93±0.12	9	9
1627+444	3C337	0.635	26.70	337±4	5.0±0.9	6.08±0.19	30	30
1658+302	B2	0.0351	23.39	120±10	2.2±0.2	5.47±0.07	21	20
1723+510	3C356	1.079	26.96	643±13	7.9±1.0	6.55±0.10	9	9
1726+318	3C357	0.1664	25.43	395±10	3.0±0.6	6.76±0.16	21,3	20
1957+405	CygA	0.0564	27.25	185±3	3.8±0.5	5.57±0.11	9	9
2019+098	3C411	0.467	27.05	201±5	2.6±0.6	6.00±0.18	26	26
2104+763	3C427.1	0.572	26.75	173±5	2.9±0.7	5.71±0.19	9	9
2145+151	3C437	1.48	27.43	317±9	5.9±1.0	5.86±0.19	30	30

## References

- |                                     |                                 |
|-------------------------------------|---------------------------------|
| (1) Alexander and Leahy 1987        | (16) Mack et al. 1998           |
| (2) van Breugel and Willis 1981     | (17) Myers and Spangler 1985    |
| (3) Fanti et al. 1986               | (18) Parma et al. 1986          |
| (4) Hine 1979                       | (19) Parma et al. 1996          |
| (5) Ishwara-Chandra and Saikia 1999 | (20) Parma et al. 1999          |
| (6) Klein et al. 1995               | (21) de Ruiter et al. 1986      |
| (7) Lara et al. 2000                | (22) Saripalli et al. 1994      |
| (8) Leahy and Williams 1984         | (23) Schoenmakers et al. 1998   |
| (9) Leahy et al. 1989               | (24) Schoenmakers et al. 2000   |
| (10) Liu et al. 1992                | (25) Schoenmakers et al. 2001   |
| (11) Machalski and Condon 1983      | (26) Spangler and Pogge 1984    |
| (12) Machalski and Condon 1985      | (27) FIRST (Becker et al. 1996) |
| (13) Machalski and Jamrozy 2000     | (28) NVSS (Condon et al. 1998)  |
| (14) Machalski et al. 2001          | (29) this paper                 |
| (15) Mack et al. 1997               | (30) Guerra et al. 2000         |

Table 2: Age and physical parameters

Source	t [Myr]	$\lg u_{\text{eq}}$ [Jm <sup>-3</sup> ]	$B_{\text{eq}}$ [nT]	$\lg U_{\text{eq}}$ [J]	$\lg Q_0$ [W]	$\lg \rho_0$ [kgm <sup>-3</sup> ]	$\lg p_c$ [Nm <sup>-2</sup> ]	$\frac{2Q_0 t}{U_{\text{eq}}}$
GIANTS								
0109+492	96±18	-13.74 ± 0.12	0.14±0.02	52.81±0.28	37.69	-24.03	-13.86	4.6±2.0
0136+396	89±17	-13.24 ± 0.17	0.25±0.05	53.14±0.31	38.29	-23.30	-13.36	8.0±4.2
0313+683	140±24	-14.11 ± 0.14	0.09±0.02	52.91±0.23	37.82	-23.87	-14.11	7.2±2.6
0319-454	180±40	-13.83 ± 0.13	0.13±0.02	53.62±0.28	38.07	-23.79	-14.15	3.2±1.3
0437-244	19±6	-12.37 ± 0.15	0.68±0.12	53.28±0.29	39.20	-23.37	-12.46	10.0±3.5
0813+758	84±4	-13.60 ± 0.15	0.17±0.03	53.47±0.22	38.47	-23.90	-13.79	5.3±2.5
0821+695	84±10	-13.37 ± 0.17	0.21±0.04	53.87±0.30	38.84	-23.68	-13.64	5.0±2.8
1003+351	127±18	-14.25 ± 0.14	0.08±0.01	53.42±0.27	38.62	-23.83	-14.34	12.8±6.1
1025-229	64±12	-12.82 ± 0.22	0.40±0.10	53.19±0.31	38.23	-23.25	-13.10	4.4±2.3
1209+745	110±20	-13.79 ± 0.13	0.13±0.02	52.93±0.28	37.60	-24.23	-13.99	5.3±1.5
1232+216	22±3	-12.29 ± 0.32	0.74±0.27	53.37±0.43	39.20	-23.20	-12.38	9.4±8.0
1312+698	55±5	-13.44 ± 0.14	0.19±0.03	52.74±0.29	37.95	-23.97	-13.56	5.7±3.2
1343+379	94±16	-14.20 ± 0.33	0.08±0.03	53.07±0.41	38.24	-24.16	-14.25	8.8±6.8
1349+647	16±4	-11.84 ± 0.17	1.25±0.25	54.03±0.33	39.79	-23.30	-12.07	5.8±3.0
1358+305	125±25	-13.95 ± 0.14	0.12±0.02	53.58±0.30	38.34	-24.12	-14.10	4.6±2.2
1543+845	130±21	-13.46 ± 0.23	0.19±0.05	53.01±0.35	38.03	-23.00	-13.61	8.6±5.6
1550+202	134±27	-13.63 ± 0.27	0.16±0.05	53.24±0.36	38.26	-23.21	-13.73	8.9±5.7
2043+749	64±11	-13.57 ± 0.10	0.17±0.02	53.04±0.23	38.14	-24.06	-13.74	5.1±1.9
NORMAL								
0154+286	13±2	-11.55 ± 0.16	1.74±0.32	53.46±0.32	39.43	-22.98	-11.72	7.7±5.0
0229+341	11±2	-11.31 ± 0.19	2.31±0.43	53.65±0.35	39.69	-22.91	-11.33	7.8±5.4
0231+313	4.6±0.3	-10.71 ± 0.16	4.58±0.85	53.62±0.29	39.64	-23.55	-11.03	3.2±1.9
0404+428	18±3	-11.91 ± 0.17	1.15±0.23	53.08±0.30	39.02	-22.96	-12.01	10.2±5.5
0610+260	45±4	-11.72 ± 0.18	1.43±0.30	53.47±0.36	39.00	-22.20	-11.54	10.2±7.6
0640+233	60±10	-12.34 ± 0.16	0.70±0.13	53.03±0.32	38.33	-22.66	-12.30	7.9±4.5
0642+214	14±5	-11.71 ± 0.22	1.44±0.37	52.58±0.34	38.87	-22.71	-11.23	17.9±7.9
0710+118	35±5	-11.54 ± 0.16	1.76±0.32	53.57±0.34	39.09	-22.31	-11.52	7.8±5.0
0806+426	7.0±1.2	-10.46 ± 0.12	6.13±0.82	53.22±0.33	39.27	-22.56	-10.57	5.0±2.3
0828+324	59±9	-13.27 ± 0.18	0.24±0.05	51.90±0.27	37.20	-23.60	-13.24	7.8±3.6
0908+376	28±5	-12.33 ± 0.16	0.71±0.13	51.38±0.23	36.83	-23.36	-12.39	5.5±2.0
0958+290	22±4	-12.11 ± 0.15	0.92±0.16	52.94±0.30	38.53	-23.31	-12.32	5.7±2.9
1008+467	2.8±0.3	-10.28 ± 0.16	7.48±1.39	53.20±0.35	39.66	-23.21	-10.36	5.5±4.0
1012+488	38±6	-12.83 ± 0.13	0.40±0.06	53.40±0.23	38.81	-23.93	-12.80	6.7±2.6
1030+585	14±2	-11.56 ± 0.16	1.72±0.32	53.01±0.33	38.98	-22.84	-11.62	8.9±5.5
1056+432	3.2±0.3	-10.72 ± 0.14	4.55±0.71	52.75±0.31	39.18	-23.44	-10.81	5.7±3.5
1100+772	32±6	-11.92 ± 0.16	1.14±0.21	52.76±0.38	38.24	-22.87	-11.95	6.5±4.6
1111+408	3.1±0.2	-10.75 ± 0.15	4.40±0.76	52.94±0.24	39.20	-23.79	-10.97	3.8±1.9
1113+295	19±3	-12.42 ± 0.16	0.64±0.12	51.25±0.26	36.84	-23.84	-12.51	5.0±2.2
1140+223	1.7±0.6	-9.87 ± 0.11	12.0±1.50	52.80±0.24	39.38	-23.27	-10.02	4.4±1.0
1141+354	3.4±0.8	-10.69 ± 0.16	4.68±0.87	52.71±0.26	39.03	-23.44	-10.85	4.8±2.4
1142+318	22±5	-11.66 ± 0.16	1.54±0.29	53.69±0.37	39.64	-22.52	-11.57	13.0±8.1
1143+500	1.2±0.5	-9.67 ± 0.16	15.1±2.80	52.22±0.23	39.32	-22.65	-9.58	10.0±4.2

Source	t [Myr]	$\lg u_{\text{eq}}$ [Jm <sup>-3</sup> ]	$B_{\text{eq}}$ [nT]	$\lg U_{\text{eq}}$ [J]	$\lg Q_0$ [W]	$\lg \rho_0$ [kgm <sup>-3</sup> ]	$\lg p_c$ [Nm <sup>-2</sup> ]	$\frac{2Q_0 t}{U_{\text{eq}}}$
1147+130	12±4	-11.10 ± 0.14	2.93±0.48	53.55±0.26	39.51	-22.60	-11.16	7.7±2.4
1157+732	13±3	-11.17 ± 0.16	2.70±0.49	53.77±0.27	39.73	-22.73	-11.20	7.8±3.2
1206+439	3.0±0.3	-10.34 ± 0.12	7.00±1.00	52.98±0.20	39.52	-23.04	-10.32	7.1±2.6
1216+507	50±15	-13.11 ± 0.18	0.29±0.06	52.75±0.28	37.98	-23.73	-13.29	5.8±1.9
1218+339	3.9±1.1	-10.35 ± 0.17	6.90±1.35	53.26±0.30	39.60	-23.00	-10.41	5.7±2.4
1221+423	18±8	-11.94 ± 0.16	1.12±0.21	53.41±0.36	39.25	-23.26	-11.90	8.1±3.1
1241+166	4.2±0.4	-11.40 ± 0.16	2.07±0.38	52.73±0.30	39.01	-24.21	-11.44	5.5±3.3
1254+476	2.8±0.3	-10.68 ± 0.16	4.77±0.88	53.08±0.25	39.59	-23.64	-10.69	6.2±2.9
1308+277	60±9	-12.60 ± 0.18	0.52±0.11	52.88±0.31	38.37	-22.59	-12.63	12.6±7.2
1319+428	110±20	-12.77 ± 0.16	0.43±0.08	52.03±0.30	37.15	-22.79	-12.90	9.1±4.9
1343+500	4.0±0.5	-10.71 ± 0.16	4.61±0.85	52.76±0.22	39.17	-23.28	-10.67	7.0±2.7
1347+285	21±4	-12.31 ± 0.13	0.73±0.11	51.13±0.22	36.35	-23.85	-12.72	2.4±0.8
1404+344	2.8±0.2	-10.59 ± 0.16	5.23±0.97	53.00±0.34	39.72	-23.15	-10.50	9.8±6.7
1420+198	43±6	-12.27 ± 0.14	0.76±0.12	53.31±0.39	38.49	-23.22	-12.47	4.4±3.3
1441+262	77±13	-13.30 ± 0.19	0.23±0.05	51.46±0.35	36.49	-23.40	-13.46	5.6±3.5
1522+546	43±7	-12.33 ± 0.15	0.71±0.12	52.82±0.30	38.07	-23.13	-12.49	5.1±2.7
1533+557	7.3±0.6	-11.00 ± 0.16	3.28±0.60	53.62±0.30	39.82	-23.01	-10.99	7.9±4.7
1547+215	3.4±1.0	-10.08 ± 0.18	9.44±1.89	53.02±0.40	39.45	-22.62	-10.19	5.8±4.1
1549+628	5.5±1.5	-10.55 ± 0.15	5.50±0.90	52.91±0.47	39.34	-22.47	-10.51	9.3±4.8
1609+660	20±3.5	-11.39 ± 0.18	2.10±0.43	53.37±0.31	39.35	-22.19	-11.36	12.9±7.1
1609+312	12±3	-12.08 ± 0.14	0.95±0.15	50.80±0.23	36.42	-24.00	-12.39	3.3±1.0
1615+324	47±9	-12.24 ± 0.15	0.79±0.14	52.25±0.34	37.78	-22.40	-12.18	10.8±6.3
1618+177	32±4	-11.91 ± 0.15	1.15±0.20	53.49±0.26	38.83	-23.10	-12.07	4.7±2.2
1627+444	24±6.5	-11.35 ± 0.13	2.20±0.32	53.23±0.37	39.03	-22.12	-11.33	9.6±4.0
1658+302	48±9	-13.05 ± 0.17	0.31±0.06	50.89±0.20	36.10	-23.67	-13.12	5.2±1.5
1723+510	20±3	-11.54 ± 0.18	1.76±0.36	53.48±0.27	39.55	-22.29	-11.53	16.0±7.7
1726+318	27±5	-12.48 ± 0.14	0.60±0.10	52.75±0.29	38.14	-23.76	-12.67	4.5±2.1
1957+405	13±3	-10.39 ± 0.15	6.60±1.18	53.64±0.25	39.39	-22.03	-10.61	4.7±1.6
2019+098	9.2±1.2	-11.14 ± 0.10	2.80±0.32	53.33±0.27	39.28	-23.20	-11.22	5.6±2.7
2104+763	7.7±0.6	-10.87 ± 0.14	3.80±0.63	53.31±0.31	39.06	-23.28	-11.25	2.9±1.9
2145+151	6.4±1.1	-10.75 ± 0.13	4.38±0.64	53.61±0.38	39.87	-22.70	-10.90	7.4±3.9

Table 3: Observational and model parameters characterizing the source's cocoon

Parameter	Symbol	Dimension
OBSERVATIONAL PARAMETERS FROM RADIO MAPS AND SPECTRA		
Apparent (projected) linear size	$D$	[kpc]
axial ratio	$AR$	[dimensionless]
observed volume	$V_0$	[kpc <sup>3</sup> ]
1.4-GHz luminosity	$P_{1.4}$	[W Hz <sup>-1</sup> sr <sup>-1</sup> ]
source redshift	$z$	[dimensionless]
PHYSICAL PARAMETERS DERIVED DIRECTLY FROM THE ABOVE DATA		
equipartition magnetic field strength	$B_{\text{eq}}$	[nT]
equipartition energy density	$u_{\text{eq}}$	[J m <sup>-3</sup> ]
equipartition emitted energy	$U_{\text{eq}} \equiv u_{\text{eq}}V_0$	[J]
PHYSICAL PARAMETERS ASSUMED IN THE MODEL		
Central core radius	$a_0$	[kpc]
exponent of density profile	$\beta$	[dimensionless]
exponent of particle energy distribution	$p$	[dimensionless]
ratio of jet-head to cocoon pressure	$\mathcal{P}_{\text{hc}} \equiv p_{\text{h}}/p_{\text{c}}$	[dimensionless]
adiabatic indices of ambient medium, cocoon, and magnetic field, respectively	$\Gamma_{\text{x}}, \Gamma_{\text{c}}, \Gamma_{\text{B}}$	[dimensionless]
source axis inclination	$\theta$	[°]
PHYSICAL PARAMETERS FITTED WITH THE MODEL FOR A GIVEN AGE		
Jet (constant) power	$Q_0$	[W]
central core density	$\rho_0$	[kg m <sup>-3</sup> ]
cocoon pressure	$p_{\text{c}}$	[N m <sup>-2</sup> ]
energy density	$u_{\text{c}}$	[J m <sup>-3</sup> ]
total emitted energy	$E_{\text{tot}} \equiv u_{\text{c}}V_{\text{c}}$	[J]

Table 4: The correlations between (log)  $D$  and  $t$  or  $Q_0$  or  $\rho_0$  when other parameters are kept constant

Correlation	$r_{XY}$	$r_{XY/U}$	$P_{XY/U}$	$r_{XY/UVW}$	$P_{XY/UVW}$
		$r_{XY/V}$	$P_{XY/V}$		
		$r_{XY/W}$	$P_{XY/W}$		
$D - t/Q_0$	+0.804	+0.941	$\ll 0.001$		
$D - t/\rho_0$		+0.805	$\ll 0.001$		
$D - t/1+z$		+0.839	$\ll 0.001$		
$D - t/Q_0, \rho_0, 1+z$				+0.952	$\ll 0.001$
$D - Q_0/\rho_0$	-0.065	+0.015	0.898		
$D - Q_0/t$		+0.810	$\ll 0.001$		
$D - Q_0/1+z$		+0.450	0.001		
$D - Q_0/\rho_0, t, 1+z$				+0.866	$\ll 0.001$
$D - \rho_0/Q_0$	-0.211	-0.256	0.031		
$D - \rho_0/t$		-0.080	0.505		
$D - \rho_0/1+z$		-0.125	0.298		
$D - \rho_0/Q_0, t, 1+z$				-0.716	$\ll 0.001$

Table 5: The correlations between (log)  $P_{1.4}$  and  $t$  or  $Q_0$  or  $1+z$  when other parameters are kept constant

Correlation	$r_{XY}$	$r_{XY/U}$	$P_{XY/U}$	$r_{XY/UV}$	$P_{XY/UV}$
		$r_{XY/V}$	$P_{XY/V}$		
$P_{1.4} - t/Q_0$	-0.718	-0.647	0.001		
$P_{1.4} - t/1+z$		-0.351	0.002		
$P_{1.4} - t/Q_0, 1+z$				-0.623	0.005
$P_{1.4} - Q_0/t$	+0.940	+0.926	$\ll 0.001$		
$P_{1.4} - Q_0/1+z$		+0.854	$\ll 0.001$		
$P_{1.4} - Q_0/t, 1+z$				+0.900	$\ll 0.001$
$P_{1.4} - (1+z)/Q_0$	+0.771	+0.270	0.023		
$P_{1.4} - (1+z)/t$		+0.515	$< 0.001$		
$P_{1.4} - (1+z)/Q_0, t$				-0.153	0.21

Table 6: The correlations between (log)  $AR$  and  $t$  or  $Q_0$  or  $\rho_0$  when the other parameters are kept constant

Correlation	$r_{XY}$	$r_{XY/U}$	$P_{XY/U}$		
		$r_{XY/V}$	$P_{XY/V}$		
		$r_{XY/W}$	$P_{XY/W}$	$r_{XY/UVW}$	$P_{XY/UVW}$
$AR - t/Q_0$	+0.328	+0.615	$\ll 0.001$		
$AR - t/\rho_0$		+0.445	<0.001		
$AR - t/1+z$		+0.488	<0.001		
$AR - t/Q_0, \rho_0, 1+z$				+0.513	<0.001
$AR - Q_0/t$	+0.235	+0.570	$\ll 0.001$		
$AR - Q_0/\rho_0$		+0.121	0.314		
$AR - Q_0/1+z$		+0.445	<0.001		
$AR - Q_0/t, \rho_0, 1+z$				+0.421	<0.001
$AR - \rho_0/t$	+0.225	+0.380	0.001		
$AR - \rho_0/Q_0$		+0.182	0.129		
$AR - \rho_0/1+z$		+0.301	0.011		
$AR - \rho_0/t, Q_0, 1+z$				+0.209	0.085

Table 7: The correlation between (log)  $p_c$  and  $D$  or  $t$  or  $1+z$  where the other parameters are kept constant

Correlation	$r_{XY}$	$r_{XY/U}$	$P_{XY/U}$		
		$r_{XY/V}$	$P_{XY/V}$		
				$r_{XY/UV}$	$P_{XV/UV}$
$p_c - D/t$	-0.792	-0.234	0.051		
$p_c - D/1+z$		-0.806	$\ll 0.001$		
$p_c - D/t, 1+z$				-0.533	<0.001
$p_c - t/D$	-0.917	-0.772	$\ll 0.001$		
$p_c - t/1+z$		-0.826	$\ll 0.001$		
$p_c - t/D, 1+z$				-0.467	0.001
$p_c - (1+z)/D$	+0.785	+0.733	$\ll 0.001$		
$p_c - (1+z)/t$		+0.145	0.23		
$p_c - (1+z)/D, t$				+0.324	0.005